
Federated Learning with Dynamic Client Arrival and Departure: Convergence and Rapid Adaptation via Initial Model Construction

Zhan-Lun Chang¹ Dong-Jun Han² Seyyedali Hosseinalipour³

Mung Chiang¹ Christopher G. Brinton¹

¹Purdue University ²Yonsei University ³University at Buffalo, SUNY

{chang837, chiang, cgb}@purdue.edu

djh@yonsei.ac.kr

alipour@buffalo.edu

Abstract

Most federated learning (FL) approaches assume a fixed client set. However, real-world scenarios often involve clients dynamically joining or leaving the system based on their needs or interest in specific tasks. This dynamic setting introduces unique challenges: (1) the optimization objective evolves with the active client set, unlike traditional FL with a static objective; and (2) the current global model may no longer serve as an effective initialization for subsequent rounds, potentially hindering adaptation. To address these challenges, we first provide a convergence analysis under a non-convex loss with a dynamic client set, accounting for factors such as gradient noise, local training iterations, and data heterogeneity. Building on this analysis, we propose a model initialization algorithm that enables rapid adaptation to new client sets whenever clients join or leave the system. Our key idea is to compute a weighted average of previous global models, guided by gradient similarity, to prioritize models trained on data distributions that closely align with the current client set, thereby accelerating recovery from distribution shifts. This plug-and-play algorithm is designed to integrate seamlessly with existing FL methods, offering broad applicability in practice. Experimental results on diverse datasets including both image and text domains, varied label distributions, and multiple FL algorithms demonstrate the effectiveness of the proposed approach across a range of scenarios.

1 Introduction

Federated learning (FL) is a decentralized machine learning paradigm that facilitates collaborative model training across multiple clients, such as smartphones and Internet of Things (IoT) clients, without exchanging individual data. Instead of transmitting raw data to the central server, each client performs local training using its proprietary data, sending only model updates to the server. These updates are then aggregated to refine the global model. In conventional FL frameworks, the cohort of clients engaged in training is typically static, implying the objective function is also fixed.

Motivation: However, in practical FL systems, the dynamic nature of client arrival and departure presents significant challenges to maintaining a robust and accurate model. For instance, clients may lose interest when their local data no longer aligns with the central task, such as when a user's application shifts from text predictions to image recognition. On the other hand, clients may join when their current objectives align with those of other clients, such as when multiple users are working with similar data types or models addressing the same problem, like medical institutions collaborating on disease detection models. Additional factors, such as evolving privacy policies,

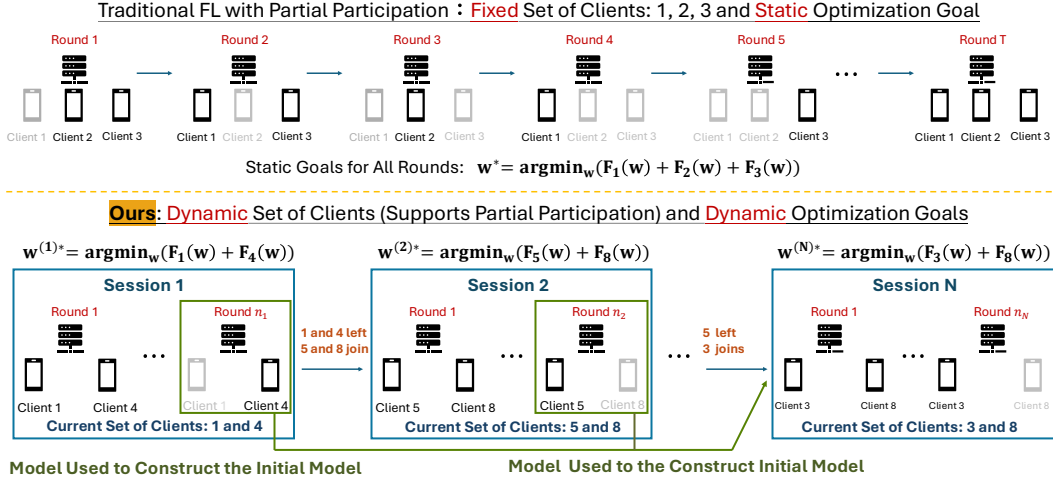


Figure 1: Comparison between traditional FL with partial participation [1–6] and our proposed dynamic FL framework. Traditional FL approaches assume a fixed client set and a static optimization goal, even when some clients are intermittently available. In contrast, our framework handles dynamic client arrivals and departures, where the optimization goal evolves to minimize the loss for the current client set in each session. A key innovation of our approach is the construction of an adaptive initial model for each session, leveraging a weighted averaging strategy guided by gradient similarity. This initial model prioritizes contributions from clients whose data characteristics align closely with the current set, facilitating efficient adaptation and mitigating the impact of client dynamics. Traditional FL with full client availability is treated as a special case of the static, partial-participation setting in this comparison.

or shifts in data-sharing preferences, further exacerbate these arrival and departure fluctuations, complicating the overall learning process.

Key Challenges: This dynamic FL setting introduces new challenges that are not present in traditional static FL scenarios with a fixed objective function. Specifically, the arrival and departure of clients dynamically alter the FL system’s objective, as the model must adapt to the current client set and their associated tasks. For instance, if a client contributing unique data classes withdraws, the model no longer needs to classify those classes, fundamentally altering the training objective. Conversely, the addition of clients with previously unrepresented classes necessitates model adaptation to incorporate the updated classification task. Thus, the core challenge is not merely preserving the diversity of the training set but dynamically adjusting the model to align with the evolving tasks defined by the current clients in the system. To address these shifting objectives, FL systems must be designed with the ability to *rapidly adapt to the current client set*, ensuring the model remains relevant, stable, and effective as the landscape of participating clients evolves.

Illustrative Examples: Figure 1 illustrates our system model, emphasizing its departure from traditional FL with a fixed client set. In conventional FL, although some clients may temporarily become inactive, the overall optimization goal remains static, aiming to minimize the aggregated loss across all clients and converge toward a single global model w^* . Prior works typically focus on designing client sampling strategies (e.g., [6]) or modifying aggregation weights (e.g., [7]) to minimize this static global loss, without accounting for evolving client sets and objectives. In contrast, our approach introduces a session-based framework that inherently supports dynamic client patterns, where the set of active clients evolves across sessions. Instead of assuming a fixed client set throughout training, our system explicitly models client arrivals and departures at the session level. Each session optimizes a session-specific model based on the current client set, ensuring adaptability to shifting data distributions. To enhance efficiency, an initial model is constructed at the start of each session using the last global model in each previous sessions, providing a better starting point than simply resuming from the last model. Within each session, our scheme also supports partial client involvement, allowing training to proceed even when only a subset of clients is active in each round. By jointly addressing dynamic client arrivals across sessions and partial client involvement within sessions, our framework offers a more flexible and realistic approach.

Main Difference from Prior Work: Unlike existing continual learning paradigms that aim to prevent catastrophic forgetting [8–10], our work focuses on enabling *fast adaptation* to the current

data distribution. This resembles a service provider aiming to build a global model that effectively serves the clients who are currently active, motivated by scenarios (e.g., mobile/edge environments) where clients frequently join and leave. From this perspective, once a client leaves, the priority shifts to optimizing performance for the remaining users rather than preserving accuracy for those who have departed. We thus adopt a dynamic, session-centric view, emphasizing responsiveness to the active client population. In Section 6, we include class incremental learning as one of our baselines and show that its performance is much worse under our objective.

Contributions: Given the challenges introduced by the dynamic nature of client arrival and departure, this work makes the following key contributions to advance the field:

- We provide a novel theoretical analysis with a non-convex loss function, deriving an upper bound on the gradient norm to quantify performance under any pattern of client arrival and departure in dynamic FL. Our analysis considers a dynamic optimization objective, where each session aims to identify an optimized model that minimizes the loss function of the current clients, contrasting with existing literature that primarily addresses a static goal of minimizing the loss across all clients that have ever participated. The derived bound incorporates several critical factors influencing performance, including: (1) stochastic gradient noise arising from inherent randomness in local updates, (2) the number of local training iterations, which affects convergence behavior, and (3) the non-IIDness of data distribution. This comprehensive analysis offers deeper insights into the trade-offs involved in model training under dynamic client arrivals and departures.
- Building on our analysis, we propose a plug-and-play algorithm designed to address dynamic optimization goals by constructing an effective initial model for each training session. The algorithm seamlessly integrates with existing FL methods (e.g., FedAvg [11], FedProx [12], SCAFFOLD [13], and FedACG [14]) to facilitate rapid adaptation to a new client set in dynamic environments. It initializes the model as a weighted average of previous models, with weights determined by gradient similarity. By leveraging these similarities, the algorithm prioritizes models trained on clients whose data characteristics closely align with those of the current ones, thereby improving adaptation and mitigating performance drop caused by dynamic client activities.
- Experimental evaluations on diverse datasets spanning both image and text domains demonstrate significant performance gains from our algorithm, particularly in scenarios with sporadic or moderately varying client patterns, highlighting the method’s effectiveness in real-world settings.

2 Related Works

Federated learning (FL) has emerged as a prominent paradigm for distributed machine learning, enabling the collaborative training of models across decentralized data sources while preserving data privacy [11, 12, 15]. One of the foundational works introduced the Federated Averaging (FedAvg) algorithm, which remains a cornerstone of many FL systems [11]. Subsequent studies have explored various aspects of federated learning, including communication efficiency [16], robustness to adversarial attacks [17], and personalization strategies [18]. However, these approaches typically assume a fixed set of participating clients throughout the training process. Reviews of FL techniques often consider static client participation, where all clients are expected to remain available for the entire training duration [12, 15]. This assumption simplifies the modeling of convergence and performance but does not adequately capture real-world scenarios characterized by dynamic client pattern. Addressing the dynamic nature of client arrival and departure is a critical gap in the current literature, motivating the need for adaptive methods that can effectively handle the entry and exit of clients during the training process.

To address the limitations of static client sets in federated learning, research on dynamic client selection and flexible participation has gained momentum, particularly in response to the challenges posed by varying client availability [3, 19–27]. These studies explore strategies such as optimizing client selection based on resource constraints, modeling participation patterns probabilistically, and employing adaptive algorithms to address the effects of non-IID data. The goal is to enhance overall model performance by strategically managing client participation during training, balancing computational efficiency, communication costs, and data representativeness. However, these works often assume a fixed client set, neglecting the dynamic nature of client arrival and departure. While [28] propose a flexible federated learning framework that allows for inactive clients, incomplete updates, or dynamic client participation, their analysis is limited to scenarios where the optimization

goal changes only once, specifically when a single client joins during training. This restricts the applicability of their approach to more complex and realistic patterns of client pattern. Also, their analysis relied on more restrictive assumptions such as strong convexity and universally bounded gradient. There is a line of work in continual FL [29, 30], where the goal is to build a model that preserves all previously learned knowledge by preventing catastrophic forgetting. In contrast, as previously mentioned, our work focuses on rapidly adapting to the current data distribution to maximize the satisfaction of clients currently active in the system. Given this difference in objectives, our approach significantly outperforms continual FL in scenarios involving dynamic client arrivals and departures, as we will see in Section 6.

3 Dynamic Federated Learning with Client Arrival and Departure

We consider a dynamic FL system where clients may join or leave the system based on their interest or task needs. Clients may join when the model aligns with their objectives, when they have sufficient new data to contribute, or when the system offers financial or computational incentives. Conversely, they may leave if the global model drifts from their needs, if they lack sufficient data, or if the model’s performance is not beneficial. Privacy or security concerns, such as adversarial threats or inadequate privacy guarantees, may also lead clients to leave. Additionally, clients may leave to allocate computational resources to other tasks or due to poor local model validation, while others may rejoin when they see improvements in these factors.

To mathematically characterize these scenarios, each round of FL training, denoted by $g \in \mathcal{G} = \{1, \dots, G\}$, involves a client set collected in $\mathcal{K}^{(g)} = \{1, \dots, K^{(g)}\}$. All clients are connected to a central server, with each client maintaining its own ML models tailored to specific tasks such as pattern recognition and natural language processing. These models are trained locally on client-specific data, allowing the system to leverage diverse data sources while preserving user privacy. At global round g , every client $k \in \mathcal{K}^{(g)}$ is linked with a dataset $\mathcal{D}_k^{(g)}$, which comprises $D_k^{(g)} \triangleq |\mathcal{D}_k^{(g)}|$ data samples. Each data sample $d \in \mathcal{D}_k^{(g)}$ includes a feature vector d and its corresponding label. A loss function $f(\mathbf{w}, d)$ evaluates the performance of parameter $\mathbf{w} \in \mathbb{R}^M$ where M represents the model’s dimensionality for each data sample $d \in \mathcal{D}_k^{(g)}$. For a specific \mathbf{w} , during the g -th global round, the local loss at client k is defined as $F_k^{(g)}(\mathbf{w}) \triangleq \sum_{d \in \mathcal{D}_k^{(g)}} \frac{f(\mathbf{w}, d)}{D_k^{(g)}}$. Then, the global loss of the ML model is given by $F^{(g)}(\mathbf{w}) \triangleq \frac{1}{D^{(g)}} \sum_{k \in \mathcal{K}^{(g)}} D_k^{(g)} F_k^{(g)}(\mathbf{w})$ where $D^{(g)} \triangleq |\mathcal{D}^{(g)}|$ is the cardinality of $\mathcal{D}^{(g)}$, the collection of data samples across clients. The main objective of training is to minimize the global loss function, which determines the model’s effectiveness in real-world downstream tasks on clients. However, dynamic client pattern, where clients may join or leave the system at any time, causes the global loss function to vary across rounds. Thus, the optimal global model parameters form a sequence $\{\mathbf{w}^{(g)*}\}_{g=1}^G$, where

$$\mathbf{w}^{(g)*} = \arg \min_{\mathbf{w} \in \mathbb{R}^M} F^{(g)}(\mathbf{w}, \mathcal{D}^{(g)}), \quad g \in \mathcal{G}. \quad (1)$$

Given this dynamic objective, the training process in round g is specifically designed to optimize the model for the data currently held by the participating clients, aiming to minimize the loss function $F^{(g)}(\mathbf{w}, \mathcal{D}^{(g)})$. Unlike continual learning, which typically aims to retain performance on previously encountered data distributions, this training strategy focuses on optimizing for the data distribution specific to the current round g . In each training round, the server broadcasts the current global model $\mathbf{w}^{(g)} \in \mathbb{R}^M$ to all clients $\mathcal{K}^{(g)}$. Upon receiving the global model, each client $k \in \mathcal{K}^{(g)}$ updates the model using its local dataset $\mathcal{D}_k^{(g)}$ over $e_k^{(g)}$ steps of stochastic gradient descent (SGD). During the h -th SGD iteration, where $h \in \{0, \dots, e_k^{(g)} - 1\}$, the update rule is given by $\mathbf{w}_k^{(g), h+1} = \mathbf{w}_k^{(g), h} - \eta^{(g)} \nabla F_k^{(g)}(\mathbf{w}_k^{(g), h}, \mathcal{B}_k^{(g)})$, where $\eta^{(g)}$ denotes the learning rate in the g -th round, and $\nabla F_k^{(g)}(\mathbf{w}_k^{(g), h}, \mathcal{B}_k^{(g)})$ is the gradient of client k ’s local loss function evaluated on the mini-batch dataset $\mathcal{B}_k^{(g)} \subset \mathcal{D}_k^{(g)}$. The mini-batch dataset is sampled from the local dataset $\mathcal{D}_k^{(g)}$ to compute the stochastic gradient. The initial model for local training is the current global model, i.e., $\mathbf{w}_k^{(g), 0} = \mathbf{w}^{(g)}$, and the final local model after training is denoted as $\mathbf{w}_k^{(g), F}$. After completing local training, clients send their final models $\mathbf{w}_k^{(g), F}$ to the server. The server aggregates these models to update the global model as $\mathbf{w}^{(g+1)} = \sum_{k \in \mathcal{K}^{(g)}} (D_k^{(g)} \mathbf{w}_k^{(g), F} / D^{(g)})$. The server initiates the next

training round by transmitting the updated global model $\mathbf{w}^{(g+1)}$ to the new client set $\mathcal{K}^{(g+1)}$. This set includes clients that joined before model aggregation and excludes those that left during the previous round. Unlike prior studies, which optimize for all potential clients, this work focuses on optimizing the model for the current set of participating clients in each round, effectively targeting $\mathbf{w}^{(g)*}$. This strategy aligns with the dynamic nature of client patterns, avoiding optimization for clients that may not rejoin. In this framework, existing clients must complete local training before leaving, while new clients can join anytime and participate in the next global round if they join after the model broadcast.

4 Theoretical Analysis

To get the insights into how the ML algorithm performs in the complex system we consider, we first analyze the performance of the local training rule as an example (similar analysis can be done for other FL algorithms), and how it inspires the design of our proposed algorithm that can be combined with any FL algorithm to reinforce the performance. We leverage two very standard assumptions [31], [32] to derive the analysis. The notation $\|\cdot\|$ denotes the two-norm.

Assumption 1 (Smoothness of Loss Functions). Local loss function $F_k^{(g)}$ is β -smooth, $\forall k \in \mathcal{K}^{(g)}, g$: $\|\nabla F_k^{(g)}(\mathbf{w}) - \nabla F_k^{(g)}(\mathbf{w}')\| \leq \beta \|\mathbf{w} - \mathbf{w}'\|$, $\forall \mathbf{w}, \mathbf{w}' \in \mathbb{R}^M$, which implies the β -smoothness of the global loss function $F^{(g)}$, $\forall g \in \mathcal{G}$.

Assumption 2 (Bounded Dissimilarity of Local Loss Functions). There exist finite constants $\zeta_1 \geq 1, \zeta_2 \geq 0$, for any set of coefficients $\{a_k \geq 0\}_{k \in \mathcal{K}^{(g)}}$, where $\sum_{k \in \mathcal{K}^{(g)}} a_k = 1$, such that $\forall g, \mathbf{w}$ $\sum_{k \in \mathcal{K}^{(g)}} a_k \|\nabla F_k^{(g)}(\mathbf{w})\|^2 \leq \zeta_1 \|\sum_{k \in \mathcal{K}^{(g)}} a_k \nabla F_k^{(g)}(\mathbf{w})\|^2 + \zeta_2$.

The parameters ζ_1 and ζ_2 , introduced in Assumption 2, quantify the degree of heterogeneity (i.e., the extent of non-i.i.d. behavior) among the datasets distributed across devices. When the datasets are fully homogeneous (i.e., i.i.d. across devices), these parameters take the values $\zeta_1 = 1$ and $\zeta_2 = 0$. However, as the heterogeneity of the data increases, both ζ_1 and ζ_2 will grow accordingly. These parameters play crucial roles in our convergence analysis, as they influence the allowable step size for SGD and the overall convergence rate of ML model training.

To further capture the heterogeneity within the local datasets of individual devices, we introduce the concept of *local data variability*.

Definition 1 (Local Data Variability). The local data variability at each device k is measured via $\Theta_k \geq 0$, which $\forall \mathbf{w}, k$ satisfies $\|\nabla f(\mathbf{w}, d) - \nabla f(\mathbf{w}, d')\| \leq \Theta_k^{(g)} \|d - d'\|$, $\forall d, d' \in \mathcal{D}_k^{(g)}$. We further define $\Theta^{(g)} = \max_{k \in \mathcal{K}^{(g)}} \{\Theta_k^{(g)}\}$.

We next obtain the convergence analysis for the non-convex loss function in the dynamic system.

Theorem 1 (Upper Bound on the Gradient Norm). Suppose each client performs local SGD updates and the server aggregates via weighted averaging. Define $e_{\max}^{(g)} = \max_{k \in \mathcal{K}^{(g)}} e_k^{(g)}$ and $e_{\min}^{(g)} = \min_{k \in \mathcal{K}^{(g)}} e_k^{(g)}$. Assuming the learning rate $\eta^{(g)}$ is less than

$$\min\left\{0.5 - ((e_{\min}^{(g)})^{-1} - 1)^2 \beta^{-1}, \sqrt{\Lambda^{(g)}} (2\beta \sqrt{(\zeta_1 + \Lambda^{(g)}) e_{\max}^{(g)} (e_{\max}^{(g)} - 1)^{-1}})\right\},$$

where $\Lambda^{(g)} < 1$ is a constant, then for any pattern of client arrivals and departures, the cumulative average of the gradient of the global loss over G rounds satisfies:

$$\begin{aligned} \frac{1}{G} \sum_{g=1}^G \mathbb{E} \|\nabla F^{(g)}(\mathbf{w}^{(g)})\|^2 &\leq \underbrace{\frac{1}{G} \sum_{g=1}^G \frac{2\mathbb{E}[F^{(g)}(\mathbf{w}^{(g)}) - F^{(g)}(\mathbf{w}^{(g+1)})]}{\eta^{(g)}(1 - \Lambda^{(g)})}}_{(a)} + \underbrace{\frac{1}{G} \sum_{g=1}^G \frac{4\beta(\Theta^{(g)})^2 \eta^{(g)}}{1 - \Lambda^{(g)}} \sum_{k \in \mathcal{K}^{(g)}} \frac{(\tilde{\sigma}_k^{(g)})^2 e_k^{(g)} D_k^{(g)} - B_k^{(g)}}{B_k^{(g)} (D_k^{(g)})^2}}_{(b)} \\ &+ \underbrace{\frac{1}{G} \left(\sum_{g=1}^G \frac{4\beta^2 (\eta^{(g)})^2}{D^{(g)} (1 - \Lambda^{(g)})} \right) \sum_{k \in \mathcal{K}^{(g)}} (e_k^{(g)} - 1) \left(1 - \frac{B_k^{(g)}}{D_k^{(g)}} \right) \frac{\Theta^{(g)} (\tilde{\sigma}_k^{(g)})^2}{B_k^{(g)}}}_{(c)} + \underbrace{\frac{1}{G} \sum_{g=1}^G 8\beta^2 (\eta^{(g)})^2 (e_{\max}^{(g)}) (e_{\max}^{(g)} - 1) \frac{\zeta_2}{1 - \Lambda^{(g)}}}_{(d)}. \end{aligned} \quad (2)$$

Proof. Please see Appendix E. □

Term (a) reflects the expected improvement in the loss function at each training stage. Terms (b) and (c) capture the negative impacts stemming from mini-batch sampling noise (controlled by batch size $B_k^{(g)}$), local data heterogeneity across clients (measured by $\Theta^{(g)}$), and the number of local SGD steps

$(e_k^{(g)})$. Term (d) accounts for the influence of the maximum number of local SGD steps ($e_{\max}^{(g)}$) and inter-client model dissimilarity (represented by ζ_2).

Inspiration from Theorem 1 for Initial Model Construction. Term (a) in the bound (2) decomposes neatly into two contributions:

$$\mathbb{E}[F^{(g)}(\mathbf{w}^{(g)}) - F^{(g)}(\mathbf{w}^{(g)*})] \quad \text{and} \quad \mathbb{E}[F^{(g)}(\mathbf{w}^{(g)*}) - F^{(g)}(\mathbf{w}^{(g+1)})].$$

The second of these arises from the update that follows round g and is beyond our control at that stage. Our algorithmic leverage lies in the first term: by constructing an initial model $\mathbf{w}_{\text{init}}^{(g)}$ aiming to satisfy

$$\mathbb{E}[F^{(g)}(\mathbf{w}_{\text{init}}^{(g)}) - F^{(g)}(\mathbf{w}^{(g)*})] \leq \mathbb{E}[F^{(g)}(\mathbf{w}^{(g)}) - F^{(g)}(\mathbf{w}^{(g)*})],$$

we directly tighten the upper bound in Theorem 1 and reduce the cumulative average gradient norm.

Algorithmic Realization via Pilot-Model Similarity Weighting. When the data distribution in round g closely matches that of a previous session, reusing that session’s final model as $\mathbf{w}_{\text{init}}^{(g)}$ naturally yields the desired reduction in Term (a). In more heterogeneous or evolving settings, however, no single past model suffices. Instead, we form

$$\mathbf{w}_{\text{init}}^{(g)} = \sum_{s < g} \alpha_s \mathbf{w}^{(s)},$$

where the weights $\{\alpha_s\}$ are determined by the similarity between each prior data distribution and the current one. We estimate similarity by computing pilot-model gradients: greater alignment of gradients indicates higher relevance and thus a larger α_s . This similarity-weighted ensemble initialization both accelerates convergence in stationary regimes and provides robust adaptation under distribution shift, directly minimizing the controllable component of our convergence bound. From this argument, it follows that our similarity-weighted warm-start strategy is agnostic to the choice of federated learning algorithm and can be seamlessly integrated into any aggregation scheme; we validate this generality by experiments in Section 6. To make this concrete, in the next section we describe how to construct the similarity weights $\{\alpha_s\}$ that underpin our warm-start strategy.

5 Dynamic Initial Model Construction for Fast Adaptation

Terminology: Algorithm 1 outlines our proposed “Dynamic Initial Model Construction” algorithm. In this context, a “session” differs from the “number of global rounds.” A new session is initiated whenever there is a change in the data distribution, such as clients joining or leaving, while the client set remains constant within a session. Each session comprises at least one global round.

Training: From Line 15 to Line 20, each client in the current set performs local model training based on either a new initial model (Line 17) or the latest model at the server (Line 19). Upon completion of local training, each client transmits its final local model to the server, where global aggregation is performed. It is worth noting that in Algorithm 1, the local model training and the global aggregation can be performed in any desired way (e.g., FedAvg, FedProx, SCAFFOLD, and FedACG). In Line 22, we only save the last global model in each session, either for pilot model computation or as components of a new initial model.

Pilot Model: As defined in Line 24, the pilot model is established upon the completion of the pilot preparation stage (the first P sessions). It is calculated as the simple average of the final global model from each of these P sessions:

$$\mathbf{w}_{\text{pilot}} = \frac{\sum_{s=0}^{P-1} \mathbf{w}^{(sT+T-1)}}{P} \triangleq \frac{\sum_{s=0}^{P-1} \mathbf{w}_s^{\text{last}}}{P} \quad (3)$$

We introduce the notation $\mathbf{w}_s^{\text{last}} \triangleq \mathbf{w}^{(sT+T-1)}$ to concisely represent the global model saved at the end of session s . These P saved global models are subsequently discarded to free memory.

Gradient Computation and Initial Model Construction: Following the pilot model preparation stage, each subsequent session s starts with a gradient computation process designed to capture the underlying data distribution. This process uses the pilot model as the initial model, $\mathbf{w}_s^{(0)} = \mathbf{w}_{\text{pilot}}$, and

Algorithm 1 Dynamic Initial Model Construction

Require: T : global rounds per session, P : pilot preparation sessions, S : total sessions ($S \geq P$), V : gradient computation global rounds.

```

1: Initialize: Random global model  $w^{(0)}$ , lists  $Q_1$  and  $Q_2$ , similarity scaling factor  $R$ .
2: for each session  $s = 0$  to  $S - 1$  do
3:   for each global round within session,  $t = 0$  to  $T - 1$  do:  $\triangleright$  Global round index:  $sT + t$ 
4:     Gradient Computation and Initial Model Construction (After computing the pilot model)
5:     if  $s \geq P$  and  $t == 0$  then:  $w_s^{(0)} \leftarrow w_{\text{Pilot}}$ 
6:       for  $v = 0$  to  $V - 1$  do
7:         for each client  $k \in \mathcal{K}^{(sT+t)}$  do
8:           Local training starting from  $w_s^{(v)}$  for  $e_k^{(sT+t)}$  steps.
9:           Send final local model to the server.
10:        Aggregate models:  $w_s^{(v+1)}$ .
11:       if  $s > P$  then
12:         Construct new initial model  $w_s^{\text{init}}$  using (5)  $\triangleright$  Initial model construction
13:         Save  $G_s \triangleq w_s^{(V-1)} - w_s^{(0)} = w_s^{(V-1)} - w_{\text{Pilot}}$  to  $Q_2$ .  $\triangleright$  Saving computed gradient
14:     Training with New Initial Model or Previous Model
15:     for each client  $k \in \mathcal{K}^{(sT+t)}$  do
16:       if  $s \geq P$  and  $t == 0$  then
17:         Local training starting from  $w_s^{\text{init}}$  for  $e_k^{(sT+t)}$  steps.  $\triangleright$  Using new initial model
18:       else
19:         Local training starting from  $w^{(sT+t)}$  for  $e_k^{(sT+t)}$  steps.  $\triangleright$  Using the latest model
20:       Send final local model to the server.
21:     Aggregate models:  $w^{(sT+t+1)}$ .
22:   if  $t == T - 1$  then: Save  $w^{(sT+t)} \triangleq w_s^{\text{last}}$  to  $Q_1$ .  $\triangleright$  Saving the last global model in each session
23:   if  $|Q_1| == P$  then
24:     Compute pilot model  $w_{\text{Pilot}}$  using (3) and delete first  $P$  saved global models.
  
```

runs V additional global rounds to obtain a final model. $w_s^{(V-1)}$ (Line 5 to Line 10). The *computed gradient* G_s is then defined as the difference $w_s^{(V-1)} - w_{\text{Pilot}}$ (Line 13):

$$G_s \triangleq w_s^{(V-1)} - w_s^{(0)} = w_s^{(V-1)} - w_{\text{Pilot}}. \quad (4)$$

This quantity is particularly useful for evaluating the similarity between different data distributions, and its value is independent of client data amount. For each session following the pilot preparation stage, only one computed gradient is retained. If at least one such gradient has been saved after the pilot stage (Line 12), the initial model for session s is constructed using only the models saved after the pilot stage.

$$w_s^{\text{init}} \triangleq \sum_{z=P}^{s-1} \alpha_{s,z} w_z^{\text{last}}, \quad \alpha_{s,z} = \frac{e^{-R\|G_s - G_z\|_2}}{\sum_{z=P}^{s-1} e^{-R\|G_s - G_z\|_2}}. \quad (5)$$

The update rule in (5) defines a weighted average of the saved models w_z^{last} , where $\alpha_{s,z}$ denotes the corresponding weight. A small difference between the past computed gradient G_z and the current gradient G_s suggests that the data distribution in the z -th session is similar to that of the current session. Since the goal of each session is to learn a model that performs well on the current data distribution, the corresponding saved model w_z^{last} serves as a suitable initialization. In such cases, a smaller $\|G_s - G_z\|_2$ yields a larger $\alpha_{s,z}$, thereby assigning more weight to w_z^{last} in (5) and making it a dominant component of the constructed initial model.

The constant R in $\alpha_{s,z}$ controls the sensitivity to gradient differences. When $R = 0$, the initial model reduces to the simple average of all saved models after the pilot preparation stage, regardless of data similarity. In contrast, as $R \rightarrow \infty$, the initial model converges to the saved model associated with the most similar data distribution.

Remark 1. Our dynamic initial model construction algorithm provides a simple, effective, and easily integrated approach compatible with any federated learning method. Although providing formal guarantees for warm-start strategies is notoriously challenging [33, 34], especially under client heterogeneity and churn, preliminary theoretical insights (Theorem 1) and extensive empirical validation in Section 6 demonstrate its practical utility. To keep the main text focused, we defer detailed discussions to the **appendix**: Appendix B covers gradient similarity, sensitivity experiments

Table 1: Performance comparison of implementing Algorithm 1 with FedProx, FedAvg, SCAFFOLD and FedACG under different label distributions for CIFAR datasets.

Dataset	Overlap	Dir(α)	FL Alg.	First Session Transition				Second Session Transition			
				Proposed	Continuous	Previous	Average	Proposed	Continuous	Previous	Average
CIFAR10	0.0	0.3	FedAvg	65.52±2.77	68.96±2.12	69.60±2.51	74.63±1.67	63.85±5.30	61.25±5.54	47.61±1.54	64.37±4.06
			FedProx	69.88±3.95	69.12±2.22	71.43±2.77	74.63±2.13	68.07±3.28	61.19±5.87	52.76±2.63	67.66±2.70
			SCAFFOLD	80.49±1.08	76.39±2.37	74.21±1.45	80.13±1.31	77.25±1.05	68.60±4.61	72.88±0.83	72.79±1.11
		FedACG	80.10±3.69	69.03±2.41	35.46±7.74	51.24±8.33	73.35±4.07	61.65±5.26	32.21±2.56	56.68±6.25	
		0.7	FedAvg	79.15±1.31	77.33±0.66	76.04±2.09	79.91±0.36	74.63±2.55	70.22±2.81	50.92±1.53	70.63±1.89
			FedProx	79.32±1.32	77.35±0.58	77.70±0.48	80.77±0.55	76.29±0.93	70.50±2.54	56.36±0.81	72.05±1.44
	SCAFFOLD		84.62±0.36	82.96±0.03	79.59±0.80	83.43±0.38	81.15±0.90	71.46±5.91	75.57±2.02	74.88±1.05	
	0.2	0.3	FedAvg	61.96±7.12	63.19±3.24	67.95±2.66	69.11±1.35	62.81±5.75	61.23±3.19	57.71±3.46	61.58±1.24
			FedProx	67.42±5.09	63.69±3.15	68.76±1.77	68.99±1.37	67.07±3.80	60.94±4.36	60.95±4.89	64.41±2.09
			SCAFFOLD	76.45±1.20	70.17±4.42	69.76±2.06	76.31±2.25	77.39±0.94	67.34±3.10	71.34±3.17	72.76±0.35
		FedACG	74.96±2.18	63.57±3.40	39.80±2.28	57.44±7.00	76.82±2.60	59.94±4.85	36.45±2.19	59.72±3.47	
		0.7	FedAvg	74.17±3.36	71.04±0.62	73.42±0.51	74.22±0.82	73.14±4.08	70.57±1.29	64.26±0.87	67.37±0.63
FedProx			75.71±0.30	70.91±0.67	73.83±0.61	73.76±1.28	76.05±1.53	70.43±1.41	66.23±1.13	69.14±1.65	
SCAFFOLD	80.21±0.38		76.19±0.68	75.92±0.42	79.58±0.62	80.75±1.08	73.19±3.29	76.24±1.06	76.29±1.36		
CIFAR 100	0.0	0.3	FedAvg	47.87±1.26	41.71±1.20	44.60±0.91	47.33±1.09	51.33±0.82	42.88±1.59	45.39±1.93	41.50±3.71
			FedProx	47.09±0.54	41.89±0.93	45.80±1.23	47.73±0.18	50.92±0.53	43.20±1.37	48.81±0.84	44.11±1.10
			SCAFFOLD	51.68±1.00	44.51±1.14	47.77±1.35	52.35±0.64	54.64±1.57	43.34±0.45	50.74±2.09	49.16±1.10
		FedACG	45.83±1.52	41.61±0.32	3.82±2.15	4.01±1.80	48.33±5.25	46.63±1.27	2.00±0.40	10.67±8.36	
		0.7	FedAvg	52.14±0.29	46.18±0.56	47.83±0.25	51.04±0.59	54.60±0.87	45.78±1.61	48.30±0.75	46.65±1.41
			FedProx	50.77±0.70	46.17±1.30	49.77±0.43	51.32±0.64	54.25±0.69	46.56±0.26	52.34±0.72	47.37±0.99
	SCAFFOLD		55.00±0.09	52.25±0.79	52.01±0.88	55.66±0.55	57.60±0.27	48.93±1.36	54.52±0.91	51.63±1.06	
	FedACG	52.97±4.84	46.29±1.05	1.82±1.49	5.91±6.76	55.38±6.27	50.71±0.46	2.59±1.47	22.75±15.49		
	0.2	0.3	FedAvg	46.95±1.24	42.03±0.28	44.78±0.61	46.11±0.63	50.29±1.53	43.41±0.94	47.26±2.04	42.89±0.67
			FedProx	46.35±0.51	42.21±0.16	45.08±0.73	47.24±0.48	50.61±0.16	43.74±1.19	48.53±0.80	44.06±0.20
			SCAFFOLD	50.20±1.16	45.94±0.79	48.23±0.49	51.01±0.84	54.04±0.73	45.23±0.73	52.18±0.84	49.08±0.27
		FedACG	56.46±0.94	42.83±0.70	20.87±0.28	34.79±5.97	57.58±0.28	44.27±0.33	22.31±2.51	41.11±4.48	
0.7		FedAvg	50.56±0.28	46.62±0.23	48.28±0.52	48.64±0.52	54.05±0.70	48.38±0.15	52.18±0.13	45.85±1.05	
		FedProx	48.90±0.57	46.60±0.41	48.33±1.52	50.24±0.42	53.12±0.82	48.24±0.41	52.41±0.83	47.99±0.95	
	SCAFFOLD	53.27±0.68	52.21±0.25	50.87±0.91	54.09±0.21	56.76±0.77	51.71±0.42	55.09±0.65	51.86±0.28		
FedACG	59.11±0.72	46.66±0.40	23.82±0.84	35.15±9.77	60.70±0.39	48.22±0.06	24.38±1.71	47.24±0.42			

on R and how well computed gradients capture the underlying data distribution, as well as ablation studies; Appendix C analyzes computation, communication and storage costs.

6 Experiments

FL Algorithm and Baselines: We evaluate the proposed initial model construction method by integrating it with established FL algorithms, including FedAvg [11], FedProx [12], SCAFFOLD [13] and FedACG [14]. Notably, FedACG represents a state-of-the-art approach that has demonstrated superior performance, surpassing methods such as FedDyn [35]. For comparative analysis, we also consider three baseline approaches: Previous, Average, and Continuous (for image dataset). The Previous baseline utilizes the model from the preceding session for continued training, foregoing the explicit construction of a dedicated initial model [11, 36–38]. The Average baseline initializes models using the unweighted average of prior global models. The Continuous baseline employs the Class-Semantic Relation Distillation Loss [29], which uses the model from the previous session as an anchor for the current client local model. This encourages the new model to preserve relationships between class representations from prior sessions while adapting to incoming client data.

Task and Dataset: We perform classification tasks on seven diverse benchmarks, including six image datasets (MNIST [39], Fashion-MNIST [40], SVHN [41], CIFAR-10 [42], CIFAR-100 [42], TinyImageNet [42]) and the AG News text corpus [43]. Results for CIFAR-10, CIFAR-100, and AG News are shown in the main text. Additional experiments appear in Appendix A.

Label Distribution: In our main experiments, we utilize 20 clients, while results with more clients (e.g. 50 or 100) are provided in Appendix A and the supplementary materials. Data samples are distributed among clients by defining the set of labels available within a training session. To introduce variation in the label distribution across the training process, the set of labels available in one training session can partially overlap with the set of labels available in a subsequent session. This overlap level can range from zero (meaning the label sets for consecutive sessions are disjoint) up to a value approaching one (meaning most labels are shared, with only a small fraction unique to each set). For the labels available in a session, they are distributed among the active clients using a Dirichlet distribution parameterized by α [11, 44–47]. A smaller value of α results in a more heterogeneous

Table 2: Performance comparison of implementing Algorithm 1 with FedProx, FedAvg, SCAFFOLD and FedACG under different label distributions for AG News text corpus.

Dataset	Overlap	Dir(α)	FL Alg.	First Session Transition			Second Session Transition		
				Proposed	Previous	Average	Proposed	Previous	Average
AG News	0.0	0.3	FedAvg	68.34±0.34	14.96±0.17	68.94±0.45	73.96±0.84	14.09±0.30	14.30±0.04
			FedProx	68.29±0.37	14.95±0.17	68.90±0.46	73.93±0.85	14.08±0.31	14.29±0.03
			SCAFFOLD	61.84±0.45	13.13±0.44	60.85±2.03	66.68±1.80	12.96±0.12	12.96±0.34
			FedACG	74.71±0.23	16.16±0.21	58.95±1.50	79.91±0.20	15.14±0.10	26.21±1.36
	0.7	FedAvg	68.37±0.38	14.95±0.17	68.96±0.48	73.93±0.81	14.11±0.31	14.30±0.03	
		FedProx	68.32±0.38	14.95±0.16	68.92±0.46	73.89±0.86	14.11±0.31	14.28±0.04	
		SCAFFOLD	61.90±0.45	13.14±0.43	60.90±2.19	66.73±1.86	12.97±0.14	12.98±0.34	
		FedACG	74.74±0.21	16.16±0.21	58.96±1.57	79.88±0.25	15.14±0.11	26.18±1.36	
	0.6	0.3	FedAvg	57.94±0.93	52.12±1.33	51.27±0.93	60.53±0.87	52.54±1.24	52.26±0.91
			FedProx	57.86±0.93	52.10±1.33	51.22±0.90	60.45±0.91	52.50±1.24	52.23±0.91
			SCAFFOLD	47.88±1.57	47.65±1.57	45.27±1.25	49.51±1.06	49.29±1.49	46.74±1.09
			FedACG	67.24±0.91	55.26±0.72	57.44±0.76	70.28±0.88	55.11±1.10	57.69±0.68
0.7	FedAvg	57.88±0.93	52.11±1.27	51.26±0.91	60.50±0.93	52.53±1.25	52.28±0.92		
	FedProx	57.82±0.95	52.09±1.28	51.22±0.88	60.45±0.94	52.51±1.26	52.25±0.92		
	SCAFFOLD	48.10±1.49	47.73±1.56	45.34±1.24	49.59±1.07	49.33±1.41	46.83±1.13		
	FedACG	67.24±0.87	55.21±0.72	57.45±0.76	70.34±0.95	55.10±1.12	57.69±0.73		

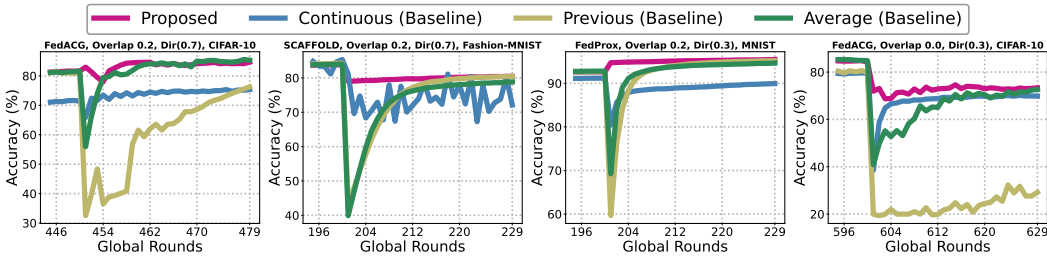


Figure 2: Performance comparison of the proposed algorithm implemented with selected FL algorithms across selected datasets. The results demonstrate the robustness of our proposed scheme to dynamic data distributions caused by client arrivals and departures.

distribution of labels across clients, leading to higher non-IIDness between clients. Conversely, a larger value of α yields a more homogeneous distribution of labels across clients.

Results and Takeaways: All values are reported as mean \pm sample standard deviation (%) over three random seeds. Table 1 and Table 2 compare the mean accuracy (\pm std) of our proposed warm start algorithm combined with several federated learning methods against the baseline aggregation schemes in the initial rounds following each session transition on CIFAR10, CIFAR100 and AG News. Across diverse datasets and label distribution scenarios, our approach consistently mitigates the accuracy drop induced by dynamic client arrivals and departures and accelerates recovery whenever the new distribution closely resembles one encountered previously. Figure 2 shows the performance of our proposed algorithm for selected setups across different datasets. It visualizes the fast recovery and robustness client arrivals and departures of our proposed algorithm.

Additional Results: We additionally evaluate our approach with a larger number of clients (e.g., 50 or 100) and on more complex datasets such as TinyImageNet in Appendix A and supplementary materials to further demonstrate its effectiveness. We also examine different label distributions and analyze the impact of the scaling factor R in the appendix and supplementary material.

7 Conclusion

This work addresses the challenges posed by dynamic client participation in FL, where clients may join or leave the system during training. We conduct a theoretical analysis under non-convex loss settings, revealing how factors such as stochastic gradient noise, local training iterations, and non-IID data distributions influence performance. Building on this analysis, we propose a plug-and-play algorithm that constructs an effective initial model for each training round using a weighted averaging strategy guided by gradient similarity. The approach integrates seamlessly with existing FL methods, prioritizing models from clients with data characteristics similar to the active clients, thereby enhancing adaptability and mitigating performance degradation. Experimental results demonstrate

significant improvements across diverse datasets and client arrival and departure patterns, underscoring the practical utility of the method in real-world FL scenarios. Future work could refine the initial model construction process to trigger updates only when necessary, reducing computational overhead while maintaining performance and enabling more efficient, adaptive FL systems.

References

- [1] Krishna Pillutla, Kshitiz Malik, Abdel-Rahman Mohamed, Mike Rabbat, Maziar Sanjabi, and Lin Xiao. Federated learning with partial model personalization. In *International Conference on Machine Learning*, pages 17716–17758. PMLR, 2022.
- [2] Jieming Bian, Lei Wang, Kun Yang, Cong Shen, and Jie Xu. Accelerating hybrid federated learning convergence under partial participation. *IEEE Transactions on Signal Processing*, 2024.
- [3] Divyansh Jhunjhunwala, Pranay Sharma, Aushim Nagarkatti, and Gauri Joshi. Fedvarp: Tackling the variance due to partial client participation in federated learning. In *Uncertainty in Artificial Intelligence*, pages 906–916. PMLR, 2022.
- [4] Haibo Yang, Minghong Fang, and Jia Liu. Achieving linear speedup with partial worker participation in non-iid federated learning. *Proceedings of ICLR*, 2021.
- [5] Shiqiang Wang and Mingyue Ji. A unified analysis of federated learning with arbitrary client participation. *Advances in Neural Information Processing Systems*, 35:19124–19137, 2022.
- [6] Wenlin Chen, Samuel Horváth, and Peter Richtárik. Optimal client sampling for federated learning. *Transactions on Machine Learning Research*, 2022. ISSN 2835-8856. URL <https://openreview.net/forum?id=8GvRCWKHIL>.
- [7] Shiqiang Wang and Mingyue Ji. A lightweight method for tackling unknown participation statistics in federated averaging. In *International Conference on Learning Representations*, 2024.
- [8] Jaehong Yoon, Wonyong Jeong, Giwoong Lee, Eunho Yang, and Sung Ju Hwang. Federated continual learning with weighted inter-client transfer. In *International Conference on Machine Learning*, pages 12073–12086. PMLR, 2021.
- [9] Wenke Huang, Mang Ye, and Bo Du. Learn from others and be yourself in heterogeneous federated learning. In *Proceedings of the IEEE/CVF conference on computer vision and pattern recognition*, pages 10143–10153, 2022.
- [10] Yuhang Ma, Zhongle Xie, Jue Wang, Ke Chen, and Lidan Shou. Continual federated learning based on knowledge distillation. In *IJCAI*, pages 2182–2188, 2022.
- [11] H. Brendan McMahan, Eider Moore, Daniel Ramage, Seth Hampson, and Blaise Aguerre y Arcas. Communication-efficient learning of deep networks from decentralized data. In *Proceedings of the 20th International Conference on Artificial Intelligence and Statistics (AISTATS)*, pages 1273–1282. PMLR, 2017.
- [12] Tian Li, Anit Kumar Sahu, Manzil Zaheer, Maziar Sanjabi, Ameet Talwalkar, and Virginia Smith. Federated optimization in heterogeneous networks. *Proceedings of Machine learning and systems*, 2:429–450, 2020.
- [13] Sai Praneeth Karimireddy, Satyen Kale, Mehryar Mohri, Sashank J Reddi, Sebastian U Stich, and Ananda Theertha Suresh. Scaffold: Stochastic controlled averaging for on-device federated learning. In *Proceedings of the 37th International Conference on Machine Learning (ICML)*, pages 5132–5143, 2020.
- [14] Geeho Kim, Jinkyu Kim, and Bohyung Han. Communication-efficient federated learning with accelerated client gradient. In *Proceedings of the IEEE/CVF Conference on Computer Vision and Pattern Recognition*, pages 12385–12394, 2024.

- [15] Peter Kairouz, H. Brendan McMahan, Brendan Avent, Aurélien Bellet, Mehdi Bennis, Arjun Nitin Bhagoji, Kallista Bonawitz, Zachary Charles, Graham Cormode, Rachel Cummings, et al. Advances and open problems in federated learning. *arXiv preprint arXiv:1912.04977*, 2019.
- [16] Qiang Yang, Yang Liu, Tianjian Chen, and Yongxin Tong. Federated machine learning: Concept and applications. In *ACM Transactions on Intelligent Systems and Technology (TIST)*, volume 10, pages 1–19. ACM, 2019.
- [17] Eugene Bagdasaryan, Andreas Veit, Yiqing Hua, Deborah Estrin, and Vitaly Shmatikov. How to backdoor federated learning. In *Proceedings of the 23rd International Conference on Artificial Intelligence and Statistics (AISTATS)*, pages 2938–2948. PMLR, 2020.
- [18] Virginia Smith, Chao-Kai Chiang, Maziar Sanjabi, and Ameet Talwalkar. Federated multi-task learning. In *Proceedings of the 31st International Conference on Neural Information Processing Systems (NeurIPS)*, pages 4424–4434. Curran Associates, Inc., 2017.
- [19] Lei Fu, Huanle Zhang, Ge Gao, and Xin Liu. Client selection in federated learning: Principles, challenges, and opportunities. *IEEE Internet of Things Journal*, 10:1–10, 2023.
- [20] Tadashi Nishio and Ryo Yonetani. Client selection for federated learning with heterogeneous resources in mobile edge. In *ICC 2019-2019 IEEE International Conference on Communications (ICC)*, pages 1–7. IEEE, 2019.
- [21] Naoki Yoshida, Tadashi Nishio, Masahiro Morikura, and Kazuaki Yamamoto. Mab-based client selection for federated learning with uncertain resources in mobile networks. In *2020 IEEE Globecom Workshops (GC Workshops)*, pages 1–6. IEEE, 2020.
- [22] Saad AbdulRahman, Hajar Tout, Amine Mourad, and Chadi Talhi. Fedmccs: Multicriteria client selection model for optimal iot federated learning. *IEEE Internet of Things Journal*, 8(6): 4723–4735, 2020.
- [23] Barbara Martini. Federated learning in dynamic and heterogeneous environments: Advantages, performances, and privacy problems. *Applied Sciences*, 14(18):8490, 2024.
- [24] Wenhao Li, Chaohong Ding, Guangwen Zhang, and Jun Li. Model agnostic federated learning with a probabilistic client selection algorithm. In *2021 IEEE International Conference on Communications Workshops (ICC Workshops)*, pages 1–6. IEEE, 2021.
- [25] Tao Lin, Lingjuan Kong, Sebastian U. Stich, and Martin Jaggi. Ensemble distillation for robust model fusion in federated learning. In *Advances in Neural Information Processing Systems (NeurIPS)*, volume 34, pages 21154–21166, 2021.
- [26] Lu Chai, Yongsheng Chen, Jiangfeng Cheng, Gendai Meng, Yongxin Wang, and Wei Zhang. Fedat: A high-performance federated learning system with asynchronous model update and temporally weighted aggregation. In *Proceedings of the 2020 IEEE 26th International Conference on Parallel and Distributed Systems (ICPADS)*, pages 1081–1088. IEEE, 2020.
- [27] Xinran Gu, Kaixuan Huang, Jingzhao Zhang, and Longbo Huang. Fast federated learning in the presence of arbitrary device unavailability. *Advances in Neural Information Processing Systems*, 34:12052–12064, 2021.
- [28] Yichen Ruan, Xiaoxi Zhang, Shu-Che Liang, and Carlee Joe-Wong. Towards flexible device participation in federated learning. In *International Conference on Artificial Intelligence and Statistics*, pages 3403–3411. PMLR, 2021.
- [29] Jiahua Dong, Lixu Wang, Zhen Fang, Gan Sun, Shichao Xu, Xiao Wang, and Qi Zhu. Federated class-incremental learning. In *Proceedings of the IEEE/CVF conference on computer vision and pattern recognition*, pages 10164–10173, 2022.
- [30] Anastasiia Usmanova, François Portet, Philippe Lalanda, and German Vega. A distillation-based approach integrating continual learning and federated learning for pervasive services. *arXiv preprint arXiv:2109.04197*, 2021.

- [31] Jianyu Wang, Qinghua Liu, Hao Liang, Gauri Joshi, and H Vincent Poor. Tackling the objective inconsistency problem in heterogeneous federated optimization. *Advances in neural information processing systems*, 33:7611–7623, 2020.
- [32] Shiqiang Wang, Tiffany Tuor, Theodoros Salonidis, Kin K Leung, Christian Makaya, Ting He, and Kevin Chan. Adaptive federated learning in resource constrained edge computing systems. *IEEE journal on selected areas in communications*, 37(6):1205–1221, 2019.
- [33] Dan Hendrycks, Kimin Lee, and Mantas Mazeika. Using pre-training can improve model robustness and uncertainty. In *International conference on machine learning*, pages 2712–2721. PMLR, 2019.
- [34] Barret Zoph, Golnaz Ghiasi, Tsung-Yi Lin, Yin Cui, Hanxiao Liu, Ekin Dogus Cubuk, and Quoc Le. Rethinking pre-training and self-training. *Advances in neural information processing systems*, 33:3833–3845, 2020.
- [35] Durmus Alp Emre Acar, Yue Zhao, Ramon Matas Navarro, Matthew Mattina, Paul N Whatmough, and Venkatesh Saligrama. Federated learning based on dynamic regularization. *arXiv preprint arXiv:2111.04263*, 2021.
- [36] Mehryar Mohri, Gary Sivek, and Ananda Theertha Suresh. Agnostic federated learning. In *International conference on machine learning*, pages 4615–4625. PMLR, 2019.
- [37] Felix Sattler, Simon Wiedemann, Klaus-Robert Müller, and Wojciech Samek. Robust and communication-efficient federated learning from non-iid data. *IEEE transactions on neural networks and learning systems*, 31(9):3400–3413, 2019.
- [38] Sashank J. Reddi, Zachary Charles, Manzil Zaheer, Zachary Garrett, Keith Rush, Jakub Konečný, Sanjiv Kumar, and Hugh Brendan McMahan. Adaptive federated optimization. In *International Conference on Learning Representations*, 2021. URL <https://openreview.net/forum?id=LkFG31B13U5>.
- [39] Yann LeCun, Léon Bottou, Yoshua Bengio, and Patrick Haffner. Gradient-based learning applied to document recognition. *Proceedings of the IEEE*, 86(11):2278–2324, 1998.
- [40] Han Xiao, Kashif Rasul, and Roland Vollgraf. Fashion-mnist: a novel image dataset for benchmarking machine learning algorithms. *arXiv preprint arXiv:1708.07747*, 2017.
- [41] Yuval Netzer, Tao Wang, Adam Coates, Alessandro Bissacco, Bo Wu, and Andrew Y Ng. Reading digits in natural images with unsupervised feature learning. *NIPS Workshop on Deep Learning and Unsupervised Feature Learning*, 2011.
- [42] Alex Krizhevsky and Geoffrey Hinton. Learning multiple layers of features from tiny images. Technical report, University of Toronto, 2009.
- [43] Xiang Zhang, Junbo Zhao, and Yann LeCun. Character-level convolutional networks for text classification. *Advances in neural information processing systems*, 28, 2015.
- [44] Yue Zhao, Meng Li, Liangzhen Lai, Naveen Suda, Damon Civin, and Vikas Chandra. Federated learning with non-iid data. *arXiv preprint arXiv:1806.00582*, 2018.
- [45] Tian Li, Shengyuan Hu, Ahmad Beirami, and Virginia Smith. Ditto: Fair and robust federated learning through personalization. In *International conference on machine learning*, pages 6357–6368. PMLR, 2021.
- [46] Qinbin Li, Yiqun Diao, Quan Chen, and Bingsheng He. Federated learning on non-iid data silos: An experimental study. In *2022 IEEE 38th international conference on data engineering (ICDE)*, pages 965–978. IEEE, 2022.
- [47] Sebastian Caldas, Sai Meher Karthik Duddu, Peter Wu, Tian Li, Jakub Konečný, H Brendan McMahan, Virginia Smith, and Ameet Talwalkar. Leaf: A benchmark for federated settings. *arXiv preprint arXiv:1812.01097*, 2018.

- [48] Tiffany Hsu, Hang Qi, and Matthew Brown. Measuring the effects of non-identical data distribution for federated visual classification. In *Proceedings of the Workshop on Federated Learning for Data Privacy and Confidentiality (NeurIPS)*, 2019.
- [49] Alireza Fallah, Aryan Mokhtari, and Asuman Ozdaglar. Personalized federated learning with theoretical guarantees: A model-agnostic meta-learning approach. In *Advances in Neural Information Processing Systems (NeurIPS)*, volume 33, pages 3557–3568, 2020.
- [50] Ya Le and Xuan Yang. Tiny imagenet visual recognition challenge. *CS 231N*, 7(7):3, 2015.
- [51] Sharon L Lohr. *Sampling: design and analysis*. Chapman and Hall/CRC, 2021.

Table 3: Performance comparison of implementing Algorithm 1 with FedProx, FedAvg, SCAFFOLD and FedACG under different label distributions for MNIST, Fashion-MNIST (FMNIST), and SVHN dataset for 20 clients.

Dataset	Overlap	Dirichlet α	FL Alg.	First Session Transition				Second Session Transition			
				Proposed	Continuous	Previous	Average	Proposed	Continuous	Previous	Average
MNIST	0.0	0.3	FedAvg	90.97±0.16	86.47±0.32	62.34±0.64	90.47±0.26	94.06±0.30	84.33±0.58	72.21±0.16	82.05±0.15
			FedProx	90.96±0.16	86.47±0.32	62.27±0.62	90.47±0.26	94.06±0.30	84.33±0.58	72.16±0.16	82.01±0.17
			SCAFFOLD	88.29±0.42	79.20±7.56	39.90±1.49	86.68±0.45	92.73±0.69	80.35±3.54	53.76±0.41	61.38±0.93
		FedACG	93.57±0.12	86.47±0.32	27.49±0.35	74.72±0.69	95.85±0.11	84.33±0.58	26.43±0.17	90.49±0.18	
		0.7	FedAvg	91.01±0.13	86.98±0.21	63.11±0.78	90.54±0.24	94.09±0.28	84.61±0.52	72.59±0.02	82.33±0.18
			FedProx	91.01±0.13	86.98±0.21	63.04±0.78	90.53±0.25	94.09±0.29	84.61±0.52	72.55±0.01	82.30±0.18
	SCAFFOLD		88.60±1.34	87.79±2.04	40.67±1.18	87.71±0.84	93.20±0.29	86.64±1.44	53.38±0.77	61.22±1.60	
	0.2	0.3	FedAvg	92.08±0.03	87.97±0.35	69.69±0.43	90.50±0.10	94.38±0.31	86.46±0.57	80.23±0.35	85.26±0.48
			FedProx	92.07±0.03	87.97±0.35	69.66±0.43	90.49±0.10	94.37±0.30	86.46±0.57	80.21±0.35	85.23±0.48
			SCAFFOLD	90.30±0.15	85.52±2.54	52.62±1.92	86.13±0.91	93.27±0.66	86.19±1.87	66.33±0.28	68.84±2.03
		0.7	FedAvg	92.13±0.06	88.28±0.34	70.44±0.44	90.62±0.08	94.41±0.27	86.74±0.52	80.53±0.28	85.48±0.44
			FedProx	92.13±0.06	88.28±0.34	70.38±0.45	90.61±0.08	94.41±0.27	86.74±0.52	80.50±0.25	85.45±0.42
SCAFFOLD			89.66±0.39	89.91±0.67	54.13±0.68	85.91±1.16	93.55±0.24	90.48±1.29	66.33±0.36	68.69±2.32	
FMNIST	0.0	0.3	FedAvg	88.16±0.13	83.95±0.54	79.52±0.61	87.95±0.26	85.06±0.12	46.06±5.63	82.70±0.18	81.63±0.66
			FedProx	88.14±0.14	83.95±0.54	79.49±0.59	87.93±0.28	85.06±0.13	46.06±5.63	82.65±0.18	81.59±0.67
			SCAFFOLD	83.94±0.07	65.52±2.17	64.28±1.37	82.68±0.34	80.05±0.33	67.19±2.81	53.47±0.19	58.81±0.55
		FedACG	91.34±0.08	83.95±0.54	65.95±0.34	75.85±0.26	87.75±0.14	46.06±5.63	52.30±0.79	84.53±0.17	
		0.7	FedAvg	88.24±0.11	84.62±0.26	79.96±0.27	88.10±0.27	85.19±0.11	54.59±4.77	82.83±0.17	81.77±0.54
			FedProx	88.23±0.12	84.62±0.26	79.94±0.27	88.08±0.27	85.18±0.10	54.59±4.77	82.81±0.17	81.75±0.56
	SCAFFOLD		83.92±0.18	79.86±0.28	64.43±0.36	82.31±0.79	80.34±0.49	72.03±3.14	52.59±0.55	58.90±1.10	
	0.2	0.3	FedAvg	85.50±0.13	82.21±0.99	79.51±0.16	85.62±0.14	84.73±0.07	70.83±0.96	81.61±0.34	79.63±0.45
			FedProx	85.48±0.14	82.21±0.99	79.45±0.14	85.59±0.12	84.72±0.08	70.83±0.96	81.55±0.34	79.65±0.46
			SCAFFOLD	80.26±0.62	67.82±5.57	67.80±0.96	76.13±0.11	79.50±0.45	71.21±6.86	58.52±0.91	57.96±2.22
		0.7	FedAvg	88.68±0.03	82.21±0.99	67.71±1.23	78.04±0.86	86.69±1.01	70.83±0.96	61.93±0.58	81.48±0.17
			FedProx	85.67±0.23	82.90±0.24	79.81±0.38	85.67±0.25	84.86±0.05	73.12±1.04	81.81±0.20	79.27±0.33
SCAFFOLD			80.79±0.40	78.60±2.68	67.97±0.77	76.83±0.17	80.07±0.33	75.83±3.23	57.41±0.31	56.79±2.21	
SVHN	0.0	0.3	FedAvg	89.43±0.43	80.34±2.95	84.37±0.36	89.46±0.92	92.69±0.08	87.43±1.24	84.04±1.15	88.79±1.74
			FedProx	89.39±0.44	80.20±3.17	84.44±0.45	89.51±0.84	92.71±0.08	87.48±1.16	84.48±1.30	89.22±1.18
			SCAFFOLD	65.52±9.48	34.74±5.37	40.04±5.91	56.61±8.63	90.07±1.02	63.16±12.07	60.46±5.96	58.08±13.35
		FedACG	92.38±0.39	80.26±3.05	26.38±5.81	26.80±5.87	93.56±0.70	87.43±1.21	25.13±15.30	56.32±18.88	
		0.7	FedAvg	89.93±0.26	83.57±1.11	85.14±0.92	89.64±0.29	92.98±0.15	88.14±0.89	83.14±3.27	87.42±3.18
			FedProx	89.84±0.33	83.60±1.11	85.27±0.92	89.71±0.29	92.97±0.17	88.12±0.87	83.68±3.74	87.54±3.35
	SCAFFOLD		79.69±0.25	51.29±6.26	47.24±6.15	72.90±7.94	91.57±0.47	79.18±2.81	71.73±5.85	75.57±4.24	
	0.2	0.3	FedAvg	92.65±0.22	83.54±1.18	22.31±3.01	29.67±9.71	93.00±0.33	88.11±0.89	23.15±8.56	54.31±14.24
			FedProx	90.33±0.43	83.84±2.31	84.83±1.52	89.32±0.59	93.07±0.06	88.46±0.71	87.80±1.12	86.26±2.24
			SCAFFOLD	75.64±4.35	44.25±1.33	56.22±3.60	72.17±1.52	89.71±0.89	76.42±5.31	76.17±4.81	74.14±6.65
		0.7	FedAvg	93.00±0.64	83.74±2.28	37.38±1.85	39.66±2.93	91.35±4.27	88.47±0.68	32.39±1.71	66.63±2.01
			FedProx	90.68±0.23	86.18±0.75	84.57±0.81	89.70±0.42	93.31±0.12	89.13±0.60	87.28±2.73	86.36±4.72
SCAFFOLD			90.69±0.23	86.16±0.79	84.94±0.82	89.81±0.38	93.28±0.10	89.12±0.60	87.68±2.56	86.48±4.78	
0.2	FedAvg	79.47±2.44	57.46±9.02	59.95±4.09	70.40±0.72	91.53±0.55	82.85±1.98	80.87±2.55	81.66±2.25		
	FedProx	93.42±0.29	86.17±0.80	34.40±1.56	41.88±3.73	94.13±0.32	89.09±0.60	33.71±4.84	62.30±9.89		

A Extended Results

A.1 Supplementary Results on Label Distributions from the Main Text

A.1.1 20 clients

Table 3 further illustrates the effectiveness of Algorithm 1 on MNIST, Fashion-MNIST and SVHN dataset for a system of 20 clients.

Table 4 further illustrates the effectiveness of Algorithm 1 on TinyImagenet dataset for a system of 20 clients.

A.1.2 100 clients

Table 5 further illustrates the effectiveness of Algorithm 1 on MNIST, Fashion-MNIST, SVHN, CIFAR-10, and CIFAR-100 dataset for a system of 100 clients.

Table 6 further illustrates the effectiveness of Algorithm 1 on TinyImagenet for a system of 100 clients.

Table 7 further illustrates the effectiveness of Algorithm 1 on AG News dataset for a system of 100 clients.

Table 4: Performance comparison of implementing Algorithm 1 with MOON, FedProx, and FedACG under different label distributions for TinyImagenet dataset for 20 clients.

Dataset	Overlap	Dirichlet α	FL Alg.	First Session Transition				Second Session Transition			
				Proposed	Continuous	Previous	Average	Proposed	Continuous	Previous	Average
TinyImagenet	0.0	0.3	MOON	62.93±0.46	53.91±0.94	52.49±1.77	61.26±0.76	61.22±2.52	55.30±0.69	56.06±0.47	57.51±1.15
			FedProx	62.01±0.32	53.78±1.00	58.90±0.38	61.69±0.44	60.91±1.42	54.74±0.72	62.27±0.71	57.23±1.37
			FedACG	64.08±0.49	53.16±0.79	35.49±8.94	54.57±0.74	62.93±0.57	54.91±0.49	21.86±4.62	48.63±1.41
		0.7	MOON	64.29±0.58	56.95±0.49	55.85±0.65	63.36±0.46	63.71±0.62	57.02±0.49	57.24±0.62	60.87±0.36
			FedProx	63.32±0.33	57.04±0.56	60.80±0.38	62.85±0.74	63.09±0.63	56.94±0.38	63.80±0.37	61.17±0.60
			FedACG	65.59±0.46	56.60±0.56	41.68±2.37	57.52±1.94	63.77±1.61	56.73±0.27	28.79±1.08	55.93±2.33
	0.2	0.3	MOON	61.69±0.68	55.14±0.76	55.63±0.84	60.71±0.75	60.20±1.59	57.48±0.64	59.48±0.55	59.13±1.08
			FedProx	60.30±0.82	55.26±0.95	57.99±0.54	60.81±0.36	59.29±2.37	57.63±0.35	62.54±0.30	58.28±0.78
			FedACG	63.20±0.49	55.40±0.77	51.86±0.54	61.09±0.57	61.78±0.88	57.42±0.62	55.46±0.62	55.05±2.20
		0.7	MOON	63.12±0.44	57.12±0.68	58.69±0.63	62.18±0.80	61.83±1.24	59.22±0.82	61.60±0.43	61.45±0.51
			FedProx	61.83±0.64	57.14±0.98	58.86±0.39	62.16±0.69	60.86±0.93	58.96±0.62	63.86±0.57	60.70±0.51
			FedACG	64.54±0.27	57.46±0.42	54.03±0.98	62.27±0.41	64.17±1.55	59.23±0.55	56.70±0.48	59.89±0.67

Table 5: Performance comparison of implementing Algorithm 1 with MOON, FedProx, SCAFFOLD and FedACG under different label distributions for MNIST, Fashion-MNIST (FMNIST), SVHN, CIFAR-10, and CIFAR-100 dataset for 100 clients.

Dataset	Overlap	Dirichlet α	FL Alg.	Second Session Transition				Fourth Session Transition			
				Proposed	Continuous	Previous	Average	Proposed	Continuous	Previous	Average
MNIST	0.0	0.3	MOON	92.04±0.24	76.92±0.34	57.82±1.23	64.19±0.85	93.08±0.17	81.93±0.42	69.35±0.75	77.92±0.72
			FedProx	92.08±0.24	76.92±0.34	58.92±1.15	66.45±0.94	92.86±0.26	81.93±0.42	70.12±0.76	79.51±0.66
			SCAFFOLD	90.69±0.42	84.30±3.26	50.36±1.91	49.97±2.04	91.95±0.39	86.39±2.63	64.93±1.35	68.55±1.45
		FedACG	93.60±0.21	76.92±0.34	60.92±0.71	71.74±0.51	94.14±0.17	81.93±0.42	70.17±0.50	82.66±0.49	
		0.7	MOON	92.07±0.24	77.33±0.41	58.26±1.18	64.78±0.77	93.09±0.17	82.17±0.37	69.65±0.69	78.30±0.59
			FedProx	92.10±0.24	77.33±0.41	59.20±1.13	66.76±0.89	92.88±0.26	82.17±0.37	70.33±0.73	79.72±0.58
	SCAFFOLD		91.18±0.46	89.12±0.77	50.85±1.74	51.03±2.03	92.31±0.27	88.76±0.84	65.27±1.18	69.68±1.32	
	0.2	0.3	MOON	92.58±0.16	80.98±0.27	70.49±0.97	72.59±0.97	93.56±0.17	84.65±0.21	79.21±0.63	82.68±0.54
			FedProx	92.61±0.15	80.98±0.27	71.42±0.89	74.21±0.93	93.27±0.18	84.65±0.21	79.71±0.65	83.52±0.47
			SCAFFOLD	91.32±0.30	86.65±3.84	64.11±1.24	61.30±2.11	92.50±0.30	87.27±1.50	75.88±0.75	75.74±0.95
		FedACG	93.98±0.14	80.98±0.27	72.61±0.66	77.79±0.65	94.48±0.10	84.65±0.21	79.45±0.42	85.73±0.35	
		0.7	MOON	92.61±0.16	81.29±0.28	70.80±0.94	73.00±0.95	93.57±0.16	84.82±0.21	79.39±0.63	82.86±0.53
FedProx			92.63±0.14	81.29±0.28	71.66±0.88	74.42±0.92	93.28±0.19	84.82±0.21	79.82±0.65	83.66±0.47	
SCAFFOLD	91.72±0.32		90.06±0.86	64.59±1.28	61.98±1.94	92.78±0.24	89.85±0.82	76.13±0.80	76.28±0.98		
FedACG	93.99±0.15	81.29±0.28	72.81±0.68	77.97±0.68	94.51±0.13	84.82±0.21	79.57±0.43	85.83±0.36			
FMNIST	0.0	0.3	MOON	83.13±0.09	59.36±0.90	77.09±0.40	77.84±0.49	84.88±0.19	64.58±0.25	79.48±0.29	80.04±0.42
			FedProx	83.19±0.08	59.36±0.90	77.74±0.37	78.57±0.50	84.22±0.21	64.58±0.25	79.90±0.32	80.52±0.46
			SCAFFOLD	77.80±0.42	65.94±5.97	47.74±0.88	47.93±1.88	79.88±0.17	74.69±4.63	53.64±0.54	60.72±0.93
		FedACG	85.10±0.22	59.36±0.90	77.61±0.25	80.44±0.38	85.82±0.07	64.58±0.25	80.01±0.31	82.22±0.35	
		0.7	MOON	83.29±0.11	60.72±0.80	77.59±0.31	78.32±0.40	84.89±0.18	65.36±0.38	79.86±0.28	80.26±0.41
			FedProx	83.33±0.13	60.72±0.80	78.16±0.35	78.93±0.43	84.29±0.15	65.36±0.38	80.28±0.34	80.72±0.38
	SCAFFOLD		78.43±0.54	68.57±4.87	47.32±1.12	48.45±1.62	80.49±0.40	70.81±7.27	53.02±0.86	61.01±1.13	
	FedACG	85.17±0.25	60.72±0.80	78.03±0.29	80.68±0.39	85.81±0.13	65.36±0.38	80.45±0.26	82.41±0.29		
	0.2	0.3	MOON	82.88±0.15	72.53±0.29	74.83±0.31	76.78±0.59	84.30±0.14	75.78±0.16	77.15±0.17	79.48±0.53
			FedProx	82.91±0.13	72.53±0.29	75.55±0.28	77.69±0.63	83.81±0.19	75.78±0.16	77.63±0.16	79.96±0.54
			SCAFFOLD	77.35±0.53	69.90±6.23	55.82±1.59	50.39±4.48	79.45±0.21	70.79±4.93	61.12±1.40	61.10±2.25
		FedACG	84.63±0.12	72.53±0.29	76.09±0.23	79.21±0.37	85.36±0.16	75.78±0.16	77.92±0.21	81.54±0.22	
0.7		MOON	83.02±0.15	73.73±0.26	75.38±0.20	77.31±0.61	84.36±0.16	76.53±0.15	77.54±0.21	79.79±0.51	
		FedProx	83.04±0.15	73.73±0.26	75.99±0.19	78.14±0.73	83.95±0.22	76.53±0.15	78.06±0.21	80.22±0.56	
	SCAFFOLD	77.88±0.54	74.14±7.98	55.77±1.46	50.02±4.42	79.85±0.21	74.03±6.67	60.69±1.26	60.68±1.80		
FedACG	84.70±0.14	73.73±0.26	76.45±0.22	79.65±0.37	85.41±0.13	76.53±0.15	78.31±0.16	81.82±0.25			
SVHN	0.0	0.3	MOON	92.98±0.08	86.82±0.75	82.65±4.35	82.32±3.62	93.69±0.13	89.13±0.27	83.80±4.06	87.56±2.06
			FedProx	91.78±0.16	86.54±0.18	86.87±2.00	88.26±0.36	92.36±0.12	87.93±0.28	89.25±1.10	90.59±0.38
			SCAFFOLD	89.70±2.57	50.14±13.22	80.23±8.59	84.29±1.56	91.54±1.28	84.76±2.61	87.11±3.05	87.71±0.63
		FedACG	93.09±0.16	86.56±0.23	80.67±2.41	86.95±2.77	93.48±0.27	87.95±0.28	75.82±10.48	90.30±1.67	
		0.7	MOON	93.21±0.18	88.72±0.33	84.88±3.19	87.03±3.18	93.95±0.13	90.37±0.21	87.69±1.98	90.44±1.50
			FedProx	92.08±0.13	87.54±0.23	87.12±1.39	88.90±0.30	92.68±0.09	88.75±0.21	89.83±0.94	90.91±0.19
	SCAFFOLD		92.06±0.61	68.61±11.01	86.32±3.01	85.88±1.23	93.13±0.45	90.40±1.04	90.28±1.10	89.47±0.86	
	FedACG	93.41±0.19	87.57±0.23	80.39±3.72	88.17±2.16	93.80±0.18	88.73±0.23	76.94±5.63	91.25±1.04		
	0.2	0.3	MOON	93.23±0.18	88.20±0.90	84.16±2.15	81.18±2.49	93.86±0.19	90.22±0.39	86.34±3.65	84.40±1.80
			FedProx	92.10±0.21	87.44±0.81	88.04±2.09	85.45±1.25	92.75±0.21	89.05±0.50	90.01±1.32	88.57±0.57
			SCAFFOLD	90.28±1.63	61.27±19.08	83.62±2.11	86.01±1.59	91.90±1.32	85.59±4.43	89.27±1.20	89.81±1.06
		FedACG	93.34±0.25	87.43±0.84	84.39±1.47	89.51±1.49	93.66±0.20	89.06±0.48	87.97±1.96	91.29±0.80	
0.7		MOON	93.54±0.24	89.92±0.32	85.92±2.37	85.59±2.71	94.24±0.19	91.20±0.22	89.17±1.73	88.30±1.71	
		FedProx	92.39±0.21	88.36±0.36	88.52±2.37	86.70±1.25	93.02±0.19	89.85±0.27	90.68±1.49	89.35±0.71	
	SCAFFOLD	92.10±0.82	75.97±8.03	87.49±1.29	86.91±0.86	93.30±0.56	89.57±1.58	90.79±0.46	90.60±0.20		
FedACG	93.64±0.24	88.38±0.36	84.67±2.49	90.33±1.14	93.97±0.23	89.88±0.27	87.79±1.84	91.85±0.63			
CIFAR-10	0.0	0.3	MOON	61.29±1.22	57.89±0.82	48.09±0.39	59.17±1.51	64.73±0.71	63.34±0.53	53.91±0.92	61.77±1.53
			FedProx	61.40±1.09	57.96±0.68	45.94±0.76	59.18±1.37	64.06±0.75	63.38±0.57	51.16±0.50	61.91±1.31
			SCAFFOLD	68.44±0.73	68.93±1.91	53.67±0.64	65.15±1.10	70.49±0.59	72.52±1.55	55.75±0.87	67.62±0.95
		FedACG	61.88±2.33	57.88±0.75	44.12±1.29	64.33±1.53	64.05±2.01	63.33±0.40	45.60±1.78	65.57±1.50	
		0.7	MOON	66.28±0.51	61.39±0.73	49.03±1.55	63.70±0.46	69.46±0.45	67.11±0.51	57.95±1.08	66.00±0.53
			FedProx	66.30±0.64	61.54±0.71	46.50±1.17	64.01±0.67	69.13±0.78	67.09±0.44	54.31±1.17	66.56±0.54
	SCAFFOLD		72.95±0.68	71.91±0.81	57.37±0.84	69.29±0.86	75.12±0.81	76.43±0.38	59.80±0.57	71.71±0.89	
	FedACG	70.35±0.80	61.46±0.74	47.91±1.35	68.17±0.50	73.23±0.60	67.09±0.41	49.10±1.29	67.73±0.33		
	0.2	0.3	MOON	54.39±1.21	51.64±0.93	51.54±1.02	53.65±0.92	59.17±1.25	57.26±0.93	56.34±0.66	56.85±0.84
			FedProx	55.26±1.80	51.74±0.88	50.40±0.99	53.29±0.80	59.97±1.44	57.42±0.74	54.30±0.96	56.91±0.68
			SCAFFOLD	67.35±0.65	63.67±3.23	52.91±1.16	62.49±0.88	69.36±0.73	68.02±2.04	54.60±1.12	65.57±0.90
		FedACG	59.33±2.61	51.48±0.88	48.80±1.07	55.33±0.99	62.01±2.09	57.31±0.67	49.07±2.10	59.35±0.73	
0.7		MOON	61.78±1.59	57.64±0.52	53.14±1.17	58.49±0.82	66.10±1.53	64.19±0.45	59.72±0.74	60.73±0.73	
		FedProx	63.81±1.31	57.73±0.50	52.35±0.95	58.70±0.71	66.36±1.13	64.24±0.44	58.05±0.72	61.36±0.66	
	SCAFFOLD	71.33±0.81	69.56±0.60	58.65±0.59	67.46±0.45	73.51±0.74	74.41±1.15	61.05±0.85	70.39±0.38		
FedACG	66.27±1.49	57.67±0.56	51.04±0.52	61.61±0.39	69.04±1.37	64.20±0.48	53.47±0.73	64.66±0.37			
CIFAR-100	0.0	0.3	MOON	38.18±0.43	32.07±0.42	38.10±0.58	34.75±0.45	41.89±0.53	38.62±0.50	44.49±0.63	38.61±0.38
			FedProx	37.79±0.37	31.95±0.36	37.05±0.85	34.16±0.40	41.55±0.34	38.65±0.57	43.55±0.94	38.08±0.57
			SCAFFOLD	44.48±0.43	45.09±0.96	43.80±0.69	40.70±0.53	48.08±0.76	50.18±0.48	49.73±0.32	44.11±0.37
		FedACG	46.66±0.28	31.96±0.28	31.38±0.77	40.49±0.87	49.69±0.47	38.68±0.38	42.63±0.67	44.33±0.77	
		0.7	MOON	40.64±0.70	35.09±0.46	39.90±0.94	36.73±0.63	44.58±0.96	41.55±0.49	45.92±1.56	40.46±0.59
			FedProx	40.42±0.46	35.15±0.51	38.29±1.45	36.47±0.50	44.01±0.60	41.60±0.50	44.66±0.96	40.57±0.54
	SCAFFOLD		47.18±0.50	46.95±0.59	46.47±0.53	42.65±0.49	50.34±0.57	50.85±0.59	52.22±0.85	46.53±0.37	
	FedACG	48.81±0.57	35.09±0.50	32.81±0.62	42.18±0.83	51.58±0.90	41.74±0.38	43.66±1.19	45.83±0.51		
	0.2	0.3	MOON	44.29±0.74	39.28±0.87	44.60±0.72	36.83±0.81	47.17±0.98	45.51±0.33	50.41±0.81	40.36±0.45
			FedProx	43.85±0.92	39.65±0.45	45.31±0.84	38.71±0.31	47.01±0.78	45.51±0.28	50.48±0.46	42.39±0.38
			SCAFFOLD	49.14±0.41	48.24±1.03	47.23±1.12	42.93±0.41	52.06±0.35	51.13±0.65	52.32±1.47	46.33±0.37
		FedACG	51.17±0.25	39.52±0.81	43.37±1.28	43.78±1.05	53.16±0.31	45.04±0.71	49.33±0.89	48.11±1.20	
0.7		MOON	46.86±0.45	42.32±0.50	46.13±0.30	39.05±0.76	50.18±0.35	47.98±0.52	52.30±0.48	42.75±0.61	
		FedProx	46.31±0.45	42.50±0.52	47.57±0.22	40.55±0.40	49.34±0.48	48.09±0.42	52.63±0.32	44.13±0.50	
	SCAFFOLD	50.91±0.79	50.95±0.71	50.99±0.44	46.96±0.45	53.82±1.07	54.19±0.50	56.22±0.20	50.67±0.40		
FedACG	52.97±0.39	42.32±0.55	44.94±0.92	47.48±0.66	55.20±0.45	48.11±0.30	51.74±0.71	51.15±0.47			

Table 6: Performance comparison of implementing Algorithm 1 with MOON, FedProx, SCAFFOLD and FedACG under different label distributions for TinyImagenet dataset for a system with 100 clients.

Dataset	Overlap	Dirichlet α	FL Alg.	First Session Transition				Second Session Transition			
				Proposed	Continuous	Previous	Average	Proposed	Continuous	Previous	Average
TinyImagenet	0.0	0.3	MOON	65.98±0.30	56.16±0.26	58.58±0.51	58.15±0.33	67.03±0.42	57.64±0.67	61.71±0.79	62.57±0.45
			FedProx	65.33±0.30	56.03±0.31	63.03±0.36	61.15±0.38	66.56±0.41	57.57±0.48	64.73±0.14	63.80±0.22
			SCAFFOLD	67.51±0.17	52.43±0.92	60.19±0.26	61.66±0.24	68.47±0.23	54.64±0.65	61.11±0.38	63.81±0.27
		FedACG	66.54±0.19	56.05±0.34	32.99±3.50	55.69±1.47	67.11±0.47	57.78±0.50	36.26±1.55	62.29±0.35	
		0.7	MOON	66.29±0.47	57.73±0.29	59.72±0.70	61.17±0.57	67.77±0.32	58.79±0.42	62.64±0.55	64.33±0.33
			FedProx	66.21±0.21	57.71±0.35	63.88±0.22	61.98±0.37	67.26±0.16	58.75±0.46	65.25±0.39	64.40±0.21
	SCAFFOLD		68.55±0.35	55.33±0.63	60.67±0.54	62.50±0.32	69.23±0.41	56.46±0.41	61.12±0.85	64.71±0.28	
	0.2	0.3	FedACG	66.71±0.43	57.74±0.29	38.89±2.21	58.76±1.20	67.84±0.28	58.78±0.41	31.27±21.23	63.96±0.30
			MOON	64.99±0.66	58.67±0.35	60.88±0.51	60.79±0.29	66.36±0.61	59.79±0.42	61.91±0.54	62.98±0.27
			FedProx	65.48±0.43	58.64±0.26	63.75±0.17	60.47±0.35	66.32±0.32	59.80±0.43	65.38±0.28	63.45±0.50
		0.7	SCAFFOLD	67.58±0.46	56.77±0.49	60.84±0.45	62.22±0.38	68.09±0.31	57.66±0.69	61.35±0.57	64.48±0.45
			FedACG	66.33±0.70	58.65±0.35	57.24±0.51	58.62±0.42	66.39±0.40	59.84±0.48	55.29±0.96	62.42±0.49
MOON			66.09±0.58	59.94±0.41	62.47±0.20	62.56±0.28	67.03±0.39	60.69±0.52	63.18±0.49	64.20±0.22	
FedProx	66.06±0.22	60.00±0.51	64.40±0.17	61.49±0.31	67.06±0.31	60.58±0.54	65.46±0.22	64.06±0.38			
SCAFFOLD	68.30±0.19	58.53±0.50	61.07±0.41	63.57±0.25	68.83±0.33	58.76±0.41	61.16±0.28	65.35±0.40			
FedACG	66.51±0.34	60.02±0.42	56.94±0.73	61.96±0.45	67.06±0.12	60.58±0.44	56.75±0.72	63.95±0.36			

Table 7: Performance comparison of implementing Algorithm 1 with MOON, FedProx, SCAFFOLD and FedACG under different label distributions for AG News dataset for 100 clients.

Dataset	Overlap	Dirichlet α	FL Alg.	First Session Transition			Second Session Transition		
				Proposed	Previous	Average	Proposed	Previous	Average
AG News	0.0	0.3	MOON	73.94±1.43	14.04±0.29	14.22±0.23	75.19±1.35	14.34±0.31	24.60±2.00
			FedProx	73.89±1.43	14.03±0.28	14.20±0.21	75.10±1.41	14.34±0.31	24.33±1.95
			SCAFFOLD	66.46±2.18	12.66±0.36	12.86±0.18	69.33±1.78	13.44±0.45	13.85±0.25
		FedACG	76.27±1.28	14.52±0.30	16.95±1.06	77.18±1.41	14.78±0.29	35.19±2.65	
		0.7	MOON	73.95±1.40	14.04±0.30	14.23±0.23	74.83±1.50	14.34±0.32	24.59±1.99
			FedProx	73.90±1.40	14.03±0.29	14.20±0.21	74.75±1.56	14.34±0.31	24.32±1.93
	SCAFFOLD		66.64±2.14	12.63±0.21	12.88±0.18	68.99±3.04	13.24±0.16	13.89±0.26	
	FedACG	76.25±1.28	14.52±0.29	16.96±1.06	76.88±1.55	14.78±0.29	35.19±2.64		
	0.8	0.3	MOON	59.15±0.66	51.98±0.85	53.36±0.85	60.78±1.19	52.97±0.83	53.94±0.97
			FedProx	59.05±0.62	51.96±0.83	53.34±0.85	60.54±1.31	52.96±0.83	53.93±0.96
			SCAFFOLD	47.26±0.62	48.35±0.39	48.58±1.07	49.11±1.25	50.09±0.52	49.48±0.96
		FedACG	63.95±0.28	52.89±0.76	55.26±0.66	65.28±0.90	53.83±0.57	55.82±0.51	
0.7		MOON	59.20±0.67	51.99±0.83	53.36±0.85	60.48±0.26	52.97±0.83	53.95±0.98	
		FedProx	59.09±0.65	51.97±0.83	53.34±0.84	60.27±0.34	52.96±0.83	53.92±0.98	
	SCAFFOLD	47.37±0.61	48.87±0.21	48.73±1.07	48.68±0.72	50.42±0.27	49.58±1.00		
FedACG	63.95±0.29	52.92±0.75	55.26±0.66	64.54±0.36	53.84±0.59	55.83±0.50			

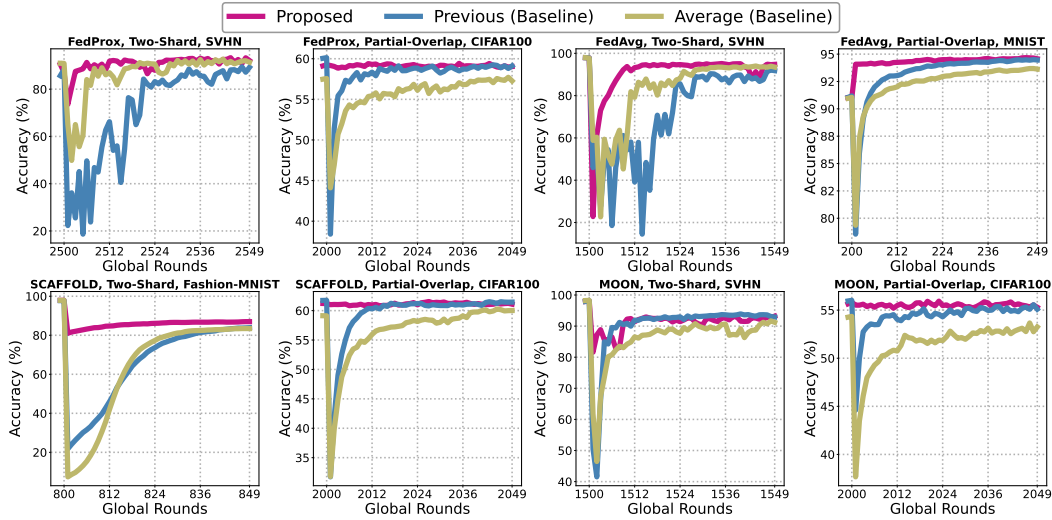


Figure 3: Performance comparison of the proposed algorithm implemented with four FL algorithms under “Two-Shard” and “Partial-Overlap” label distributions across selected datasets. The results demonstrate the robustness of our proposed scheme to dynamic data distributions caused by client arrivals and departures.

A.2 Additional Results for Alternative Label Distributions

In addition to the label distribution we used in the main text, we also evaluate Algorithm 1 using the following distribution.

- **Two-Shard** [11–13, 48, 49]: For datasets with 10 labels, each label is divided into two equally-sized shards, and each client receives two different label shards. For datasets with 100 labels, the labels are divided into 10 non-overlapping batches, and each batch is split into two shards, which are then assigned to two randomly selected clients. Each client ends up with data from two labels for 10-label datasets, or 20 labels for 100-label datasets .
- **Half**: Half the clients have one half of the labels, and the rest have the other half. Each client has all the labels from their assigned half (i.e., 5 labels for 10-label datasets or 50 labels for 100-label datasets), and the data is evenly distributed, meaning that the amount of data for each label is equally divided among the clients.
- **Partial-Overlap**: Two sets of labels are selected, each containing 60% of the total labels, with a 20% overlap between them. Each client in the first set has 6 labels for 10-label datasets (or 60 labels for 100-label datasets), and each client in the second set has a similar distribution. The overlapping labels are split between the two halves of clients, with half of the data for overlapping labels going to the first client set and the other half to the second set. The non-overlapping labels are assigned to the clients within each set, and the data corresponding to these labels is evenly distributed across the clients, meaning that each client receives an approximately equal share of the data for their assigned labels.
- **Distinct**: Each client is assigned a unique set of labels. For datasets with 10 labels, each client receives 1 unique label, while for datasets with 100 labels, each client receives 10 unique labels.

Figure 3 highlights selected scenarios and illustrates the advantages of the proposed algorithm for all FL algorithms during periods of pronounced performance drops or gains due to data distribution shifts. The algorithm prioritizes models trained on past distributions similar to the current one, enabling the initial model to adapt more quickly and consistently outperform baseline approaches. These results underscore the robustness and effectiveness of the proposed approach across diverse FL algorithms, datasets, models, and dynamic data distributions.

Table 8 compares the average accuracy of the proposed algorithm across all FL algorithms during the first 10 global rounds after three data distribution shifts under the “Two-Shard” and “Partial-Overlap” label distributions. The results across datasets, label distributions, and models show that the proposed algorithm mitigates performance degradation from dynamic client arrivals and departures. Moreover, it accelerates performance recovery when the current data distribution aligns with a previously observed one.

Table 8: Performance comparison of implementing Algorithm 1 with FedProx, FedAvg, SCAFFOLD and MOON under different label distributions and datasets. Performance is measured across 3 transitions for each dataset.

FL Algorithm	Label Distribution	Dataset (Model)	1st Transition			2nd Transition			3rd Transition		
			Proposed	Previous	Average	Proposed	Previous	Average	Proposed	Previous	Average
FedProx	Two-Shard	MNIST (MLP)	98.45	96.4	98.24	94.77	90.72	93.19	98.56	96.53	98.4
		Fashion-MNIST (MLP)	92.04	90.31	88.89	97.59	96.38	97.33	95.39	93.54	94.58
		SVHN (CNN)	86.52	40.13	72.7	97.44	84.53	95.08	95.8	55.16	83.08
		CIFAR10 (ResNet18)	41.64	35.32	39.68	46.26	35.62	44.62	82.58	58.34	78.3
		CIFAR100 (ResNet18)	58.46	56.68	51.07	49.28	46.52	47.7	52.73	48.35	51.49
	Partial-Overlap	MNIST (MLP)	62.88	56.16	56.23	64.27	57.14	53.96	63.53	57.41	56.81
		Fashion-MNIST (MLP)	87.06	83.79	86.78	88.06	85.52	84.78	87.2	84.33	86.89
		SVHN (CNN)	92.4	76.09	91.72	93.64	68.67	92.35	92.51	71.79	92.02
		CIFAR10 (ResNet18)	81.5	77.05	77.31	86.99	83.88	84.97	81.69	79.84	77.62
		CIFAR100 (ResNet18)	59.09	54.94	52.23	59.22	55.09	56.13	59.34	56.11	53.34
FedAvg	Two-Shard	MNIST (MLP)	98.45	96.4	98.24	94.77	90.72	93.19	98.56	96.53	98.4
		Fashion-MNIST (MLP)	92.04	90.31	88.89	97.59	96.38	97.33	95.39	93.54	94.58
		SVHN (CNN)	76.53	51.03	56.65	83.45	39.58	72.65	95.87	42.97	85.15
		CIFAR10 (ResNet18)	41.98	32.77	41.05	51.01	36.57	48.57	82.51	64.03	81.04
		CIFAR100 (ResNet18)	47.88	44.29	46.87	49.63	46.04	47.64	52.18	48.43	51.17
	Partial-Overlap	MNIST (MLP)	93.81	89.65	89.33	91.11	87.46	90.35	94.16	90.1	90.67
		Fashion-MNIST (MLP)	87.58	85.06	83.04	86.77	83.88	86.49	87.64	85.59	84.16
		SVHN (CNN)	92.27	79.11	89.94	93.67	82.01	91.46	92.48	77.2	91.47
		CIFAR10 (ResNet18)	85.87	82.35	83.84	79.94	77.1	75.31	85.87	82.9	84.41
		CIFAR100 (ResNet18)	56.94	53.29	54.31	57.25	54.17	51.71	57.35	54.41	54.6
SCAFFOLD	Two-Shard	MNIST (MLP)	97.97	51.69	96.73	92.27	42.16	44.86	98.32	54.78	97.26
		Fashion-MNIST (MLP)	84.24	36.59	22.94	96.89	51.82	96.18	92.29	52.41	45.45
		SVHN (CNN)	79.23	69.2	47.94	95.32	90.76	73.11	93.96	88.37	73.25
		CIFAR10 (ResNet18)	46.63	10.74	23.31	92.39	38.32	90.59	56.11	12.66	24.98
		CIFAR100 (ResNet18)	21.63	5.61	9.59	35.75	21.3	19.42	26.18	7.69	11.98
	Partial-Overlap	MNIST (MLP)	85.72	61.6	71.39	89.66	77.03	53.64	87.1	69.45	72.93
		Fashion-MNIST (MLP)	86.67	62.41	74.68	87.54	63.48	68.97	87.64	65.2	74.91
		SVHN (CNN)	90.33	84.02	73.88	91.9	89.05	80.91	91.33	85.83	74.68
		CIFAR10 (ResNet18)	72.64	37.95	42.06	79.12	39.31	69.88	74.52	40.29	49.57
		CIFAR100 (ResNet18)	61.03	52.56	48.94	61.16	53.54	58.66	60.79	53.99	53.2
MOON	Two-Shard	MNIST (MLP)	98.15	96.54	98.04	98.38	96.55	98.24	98.52	96.48	98.39
		Fashion-MNIST (MLP)	92.08	90.28	88.84	97.42	96.47	97.31	95.36	93.54	94.53
		SVHN (CNN)	87.0	78.61	75.72	69.51	64.57	54.88	93.49	90.2	89.87
		CIFAR10 (ResNet18)	44.03	40.53	39.42	51.31	43.46	41.82	85.0	71.45	73.54
		CIFAR100 (ResNet18)	57.94	56.05	44.18	45.8	43.81	44.71	62.06	60.56	53.54
	Partial-Overlap	MNIST (MLP)	93.85	89.65	89.33	91.1	87.64	90.35	94.12	90.2	90.67
		Fashion-MNIST (MLP)	87.6	85.06	83.04	86.66	83.66	86.49	88.01	85.53	84.16
		SVHN (CNN)	92.96	90.41	88.39	91.74	87.97	90.77	93.18	91.25	90.25
		CIFAR10 (ResNet18)	85.53	83.59	84.67	79.28	77.57	76.04	79.37	78.44	76.11
		CIFAR100 (ResNet18)	55.52	52.58	47.77	55.27	52.22	52.7	55.72	53.49	49.01

Table 9: Performance comparison of FedProx, FedAvg, SCAFFOLD, and MOON under “Half” and “Distinct” label distributions across various datasets. Performance is evaluated over three transitions for each dataset.

FL Algorithm	Label Distribution	Dataset (Model)	1st Transition			2nd Transition			3rd Transition		
			Proposed	Previous	Average	Proposed	Previous	Average	Proposed	Previous	Average
FedProx	Half	MNIST (MLP)	96.02	90.12	92.45	96.29	90.56	93.59	93.25	88.17	92.45
		Fashion-MNIST (MLP)	90.97	86.02	90.17	86.62	85.06	84.2	91.29	86.67	90.26
		SVHN (CNN)	93.23	27.0	92.18	91.64	17.15	90.98	93.53	69.5	92.75
		CIFAR10 (ResNet18)	86.32	48.83	83.59	90.38	54.74	87.64	87.68	58.41	84.62
	CIFAR100 (ResNet18)	62.88	56.16	56.23	64.27	57.14	53.96	63.53	57.41	56.81	
	Distinct	MNIST (MLP)	98.05	92.75	97.71	95.98	88.77	93.96	94.11	85.66	90.54
Fashion-MNIST (MLP)		95.5	92.4	95.0	95.8	90.59	94.56	94.02	87.36	90.73	
SVHN (CNN)		92.25	45.18	67.51	87.91	38.45	63.85	92.24	42.7	60.68	
FedAvg	Half	MNIST (MLP)	96.03	90.12	92.45	92.56	87.83	92.45	96.21	90.56	93.59
		Fashion-MNIST (MLP)	86.24	84.54	82.54	90.29	86.12	89.91	90.5	86.62	90.1
		SVHN (CNN)	91.63	71.49	88.78	93.54	51.98	91.07	91.98	42.34	90.55
		CIFAR10 (ResNet18)	90.19	70.15	88.08	86.23	77.41	81.67	90.03	73.55	89.25
	CIFAR100 (ResNet18)	57.41	52.95	54.37	57.09	53.7	51.07	57.48	53.38	54.44	
	Distinct	MNIST (MLP)	97.97	93.03	97.57	95.72	89.19	93.65	94.04	86.11	90.4
Fashion-MNIST (MLP)		95.81	90.66	94.44	93.88	87.5	90.56	95.8	92.0	94.86	
SVHN (CNN)		94.99	49.88	80.62	91.9	38.94	58.53	87.21	32.71	66.47	
SCAFFOLD	Half	MNIST (MLP)	85.53	29.8	82.93	92.58	57.81	30.18	89.08	51.43	84.39
		Fashion-MNIST (MLP)	77.18	36.71	28.55	83.35	65.31	77.91	79.51	40.82	42.19
		SVHN (CNN)	91.66	86.87	76.06	89.86	84.79	80.25	93.04	87.31	87.18
		CIFAR10 (ResNet18)	78.63	17.35	34.76	84.62	19.59	79.32	80.13	20.86	49.7
	CIFAR100 (ResNet18)	28.92	9.97	18.74	31.11	13.3	6.44	34.23	13.84	21.62	
	Distinct	MNIST (MLP)	96.95	50.5	95.35	93.08	22.24	60.96	91.36	21.06	22.78
Fashion-MNIST (MLP)		94.08	32.05	91.66	93.28	13.81	53.5	91.72	29.1	33.07	
MOON	Half	MNIST (MLP)	96.06	90.16	92.45	92.64	87.78	92.45	96.29	90.46	93.59
		Fashion-MNIST (MLP)	86.12	84.43	82.54	90.33	85.79	89.91	86.31	84.96	83.75
		SVHN (CNN)	93.64	89.35	89.95	92.11	87.3	91.18	93.63	90.54	91.37
		CIFAR10 (ResNet18)	89.0	85.77	88.26	84.89	81.08	81.53	89.16	86.67	88.51
	CIFAR100 (ResNet18)	54.9	52.27	53.8	55.95	52.75	48.99	55.05	52.63	54.07	
	Distinct	MNIST (MLP)	95.67	88.67	93.56	94.07	85.7	90.2	95.63	90.65	94.32
Fashion-MNIST (MLP)		95.76	90.14	94.4	93.86	86.83	90.06	95.66	91.76	94.85	

Table 9 presents a comparative analysis of the average accuracy achieved by the proposed algorithm across all federated learning (FL) algorithms during the first 10 global rounds following three shifts in data distribution under the “Half” and “Distinct” label distributions.

Table 10: Performance of Algorithm 1 with FedAvg under “Half” and “Partial-Overlap” label distributions for the TinyImageNet dataset with 20 clients. Performance is measured across three transitions for each dataset.

Label Distribution	Dataset (Model)	1st Transition		2nd Transition		3rd Transition	
		Proposed	Previous	Proposed	Previous	Proposed	Previous
Half	TinyImageNet (ResNet34)	80.72	72.81	77.77	72.24	80.43	73.42
Partial-Overlap	TinyImageNet (ResNet34)	92.27	79.11	93.67	82.01	92.48	77.2

Table 11: Performance comparison of Algorithm 1 integrated with FedProx, FedAvg, SCAFFOLD, and MOON on the MNIST and Fashion-MNIST datasets, utilizing 100 clients for FedProx, FedAvg, and MOON, and 50 clients for SCAFFOLD under the Partial-Overlap label distribution. Performance is evaluated across three transitions for each dataset.

FL Algorithm	Dataset (Model)	1st Transition			2nd Transition			3rd Transition		
		Proposed	Previous	Average	Proposed	Previous	Average	Proposed	Previous	Average
FedProx	MNIST (MLP)	94.09	89.53	89.35	91.36	87.4	90.45	94.33	89.92	90.78
	Fashion-MNIST (MLP)	87.88	85.13	83.37	87.14	83.86	86.76	88.08	85.57	84.65
FedAvg	MNIST (MLP)	90.86	86.15	90.25	94.09	89.53	89.35	91.36	87.4	90.45
	Fashion-MNIST (MLP)	86.55	82.78	86.4	87.88	85.13	83.37	87.14	83.86	86.76
SCAFFOLD	MNIST (MLP)	64.82	33.15	52.67	82.67	62.47	30.18	74.04	50.77	59.66
MOON	MNIST (MLP)	91.36	87.4	90.45	94.33	89.92	90.78	91.55	87.87	90.55
	Fashion-MNIST (MLP)	87.14	83.86	86.75	88.07	85.57	84.65	87.31	84.34	86.9

Table 10 presents the results of applying Algorithm 1 with FedAvg for 20 clients on the TinyImageNet dataset [50]. The baseline method used is “Average.” These results highlight the effectiveness of Algorithm 1 in handling scenarios with a larger client population and a more complex dataset using a more advanced model ResNet34.

Table 11 shows the results for 100 clients for Algorithm 1 integrated with FedProx, FedAvg, SCAFFOLD, and MOON on the MNIST and Fashion-MNIST datasets, using 100 clients under the Partial-Overlap label distribution. Performance is evaluated over three transitions for each dataset.

Figure 4 highlights the performance of Algorithm 1 in more selected scenarios and illustrates the advantages of the proposed algorithm for all FL algorithms during periods of pronounced performance drops or gains due to data distribution shifts. The algorithm prioritizes models trained on past distributions that share similarities with the current one, enabling the initial model to adapt more quickly to the new distribution and consistently outperforming baseline approaches. These results underscore the robustness and effectiveness of the proposed approach across diverse FL algorithms, datasets, models, and dynamic data distributions.

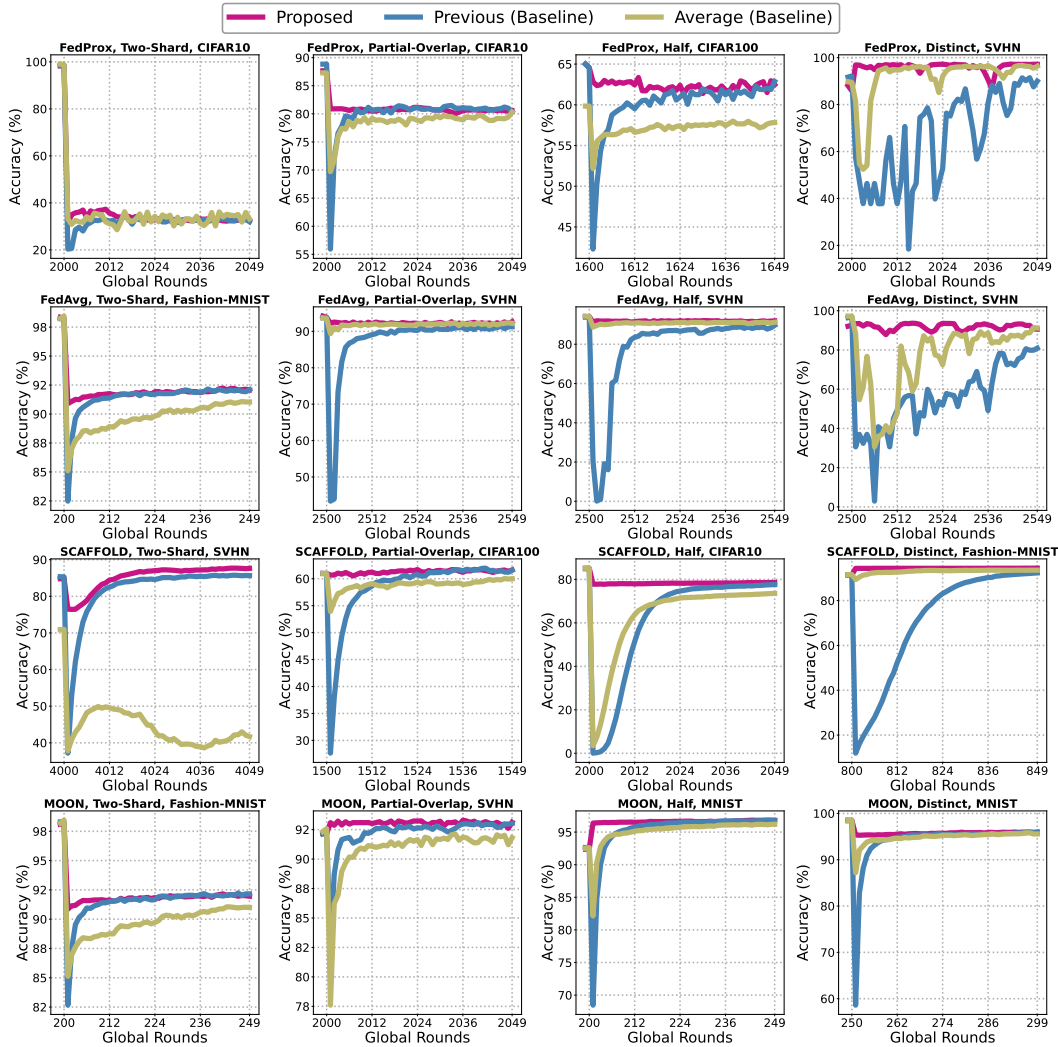


Figure 4: Performance comparison of the proposed algorithm implemented with four FL algorithms under all label distributions across more selected datasets. The results demonstrate the robustness of our proposed scheme to dynamic data distributions caused by client arrivals and departures.

B Gradient Similarity, Sensitivity Analysis and Ablation Studies for Algorithm 1

B.1 Computed Gradient and Similarity

In our method, the **computed gradient** is the *normalized global gradient* rather than any single client’s raw gradient. During aggregation, each client’s local gradient is weighted by the size of its local dataset, ensuring that clients with more data contribute proportionally more. Consequently, the global gradient captures **collective data heterogeneity** without being biased by client-size.

The utility of **gradient similarity** for model initialization depends on the alignment between current and historical data distributions. When client distributions evolve gradually and exhibit recurring patterns—a typical scenario in federated learning—gradient similarity provides an effective heuristic for selecting an initial model that adapts rapidly to new clients. While our method excels under **moderate to high overlap** conditions, completely novel classes still pose an inherent challenge in **non-stationary environments**.

To assess robustness under extreme shifts, we introduced unseen labels only in the final session and measured average test accuracy over the first ten global rounds. As shown in Table 12, our initialization strategy maintains performance comparable to baseline approaches.

Table 12: Average accuracy over the first ten rounds under the unseen-label edge case.

Algorithm	Dataset	Proposed	Previous	Average
FedAvg	Fashion-MNIST	94.98	94.75	95.89
MOON	SVHN	94.17	89.53	94.02

B.2 Sensitivity Analysis of the Similarity Scaling Factor R

We evaluate the effect of the scaling factor R in the initial-model construction (5) on both FedAvg and FedProx. Accuracy across multiple transitions remains stable for a wide range of R values.

Table 13: Sensitivity of transition performance to the similarity-scaling factor R for FedAvg and FedProx on SVHN and CIFAR-100.

Algorithm	Dataset	R	1st Transition	2nd Transition	3rd Transition
FedAvg	SVHN	50	91.78	93.49	91.87
	SVHN	80	91.76	93.58	91.90
	SVHN	100	91.63	93.54	91.98
	SVHN	120	91.80	93.59	91.83
	SVHN	140	91.77	93.47	91.75
	CIFAR-100	110	58.36	56.63	58.37
	CIFAR-100	120	56.95	56.28	57.06
	CIFAR-100	130	57.41	56.29	57.46
	CIFAR-100	140	58.30	56.37	58.42
	CIFAR-100	150	57.46	56.75	58.05
FedProx	SVHN	50	92.43	93.83	92.54
	SVHN	80	92.44	93.88	92.62
	SVHN	100	92.40	93.64	92.51
	SVHN	120	92.49	93.79	92.71
	SVHN	140	92.50	93.71	92.70
	CIFAR-100	110	58.55	58.70	58.57
	CIFAR-100	120	58.56	58.63	58.78
	CIFAR-100	130	59.02	58.50	59.06
	CIFAR-100	140	58.93	58.88	59.07
	CIFAR-100	150	59.66	59.51	59.68

B.3 Ablation Studies

We have conducted additional experiments replacing the pilot model with a **randomly initialized** one to compute gradients. Performance drops in most cases, supporting the utility of pilot model knowledge.

Table 14: Ablation study comparing the proposed pilot model versus a randomly initialized pilot across transitions and settings.

Setting	1st Transition		2nd Transition		3rd Transition	
	Proposed	Random Pilot	Proposed	Random Pilot	Proposed	Random Pilot
MOON, Two-shards, SVHN	87.00	86.03	69.51	63.14	93.49	93.32
SCAFFOLD, HALF, SVHN	91.66	71.78	89.86	87.54	93.04	84.67
FedProx, Slight Overlap, CIFAR10	81.50	79.47	86.99	86.80	81.69	79.62
MOON, Slight Overlap, SVHN	92.96	91.91	91.74	91.60	93.18	91.74

C Computation, Communication, and Storage Analysis of Algorithm 1

C.1 Cost Analysis with Variable Clients

The breakdown below provides a precise view of costs per phase. Notation follows the main text; session indexing will be refined in the revised manuscript.

Pilot Model Training (consisting of P sessions):

- *Computation:* Each of the P pilot sessions comprises T global rounds. In round g ($1 \leq g \leq T$) of a pilot session, each client $k \in \mathcal{K}^{(g)}$ executes $e_k^{(g)}$ local epochs. Total local epochs:

$$P \times \sum_{g=1}^T \sum_{k \in \mathcal{K}^{(g)}} e_k^{(g)}.$$

- *Communication:* There are $P \times T$ global rounds. In each round g , $|\mathcal{K}^{(g)}|$ clients upload updates and the server broadcasts the aggregated model. Total transmissions:

$$P \times \sum_{g=1}^T |\mathcal{K}^{(g)}| \quad (\text{client uploads}), \quad PT \quad (\text{server broadcasts}).$$

- *Storage:* Model size is W . We temporarily store P intermediate models of size W , which are discarded after constructing the pilot model.

Gradient Computation (for session s , $s \in \{P, \dots, S\}$, at global round $g = sT$):

- *Computation:* Perform V additional global rounds initialized from the pilot model. Clients in $\mathcal{K}^{(sT)}$ each run $e_k^{(sT)}$ local epochs per round, for a total of

$$V \times \sum_{k \in \mathcal{K}^{(sT)}} e_k^{(sT)}.$$

- *Communication:* Over V rounds, each round incurs $|\mathcal{K}^{(sT)}|$ uploads and one broadcast. Total:

$$V \times |\mathcal{K}^{(sT)}| \quad (\text{client uploads}), \quad V \quad (\text{server broadcasts}).$$

- *Storage:* One gradient of size W is stored for session s .

Coefficient Calculation (for session m , $m \in \{P + 1, \dots, S\}$, at $g = mT$):

- *Computation:* Computing softmax-based coefficients over the $(m - P)$ stored items incurs

$$\mathcal{O}(m - P)$$

cost for vector norms and exponentials.

Total Persistent Storage:

- *Pilot model:* One model of size W (intermediate checkpoints discarded).
- *Per post-pilot session s :*
 - Final model checkpoint: W ,
 - Computed gradient: W .
- *Overall growth:* Linear increase of $2W$ per post-pilot session, scaling with $(S - P)$.

C.2 Storage Overhead

Persistent storage grows linearly with $S - P$ (one model and one gradient per session), which remains practical.

C.3 Justification for Computation and Communication Requirements

The upfront cost of pilot training and gradient computation is offset by accelerated adaptation to shifting client distributions, reducing the total number of global rounds (e.g., avoiding 50+ recovery rounds required by standard baselines).

C.4 Mitigating Storage for Matrices Q_1 and Q_2

To bound storage growth, one may:

- *Limited history:* Retain only the most recent H sessions' models/gradients.
- *Selective retention:* Store models/gradients that maximize distributional diversity, preserving initialization quality with fewer checkpoints.

These strategies ensure manageable storage while maintaining algorithmic efficacy in dynamic federated learning settings.

D Experimental Setup, Reproducibility, and Computational Resources

D.1 Setup and Reproducibility

The following command was used to launch each experiment. The meaning and purpose of each argument are described in detail in our accompanying README.md.

```
python -u fasy_adapt_training.py \  
  --dataset_name 'cifar10' \  
  --algorithm 'scaffold' \  
  --cross_session_label_overlap 0.0 \  
  --in_session_label_dist "dirichlet" \  
  --dirichlet_alpha 0.7 \  
  --seed 300 \  
  --initial 1 \  
  --average 1 \  
  --previous 1 \  
  --continuous 0 \  
  --num_clients 100 \  
  --num_sessions 7 \  
  --num_sessions_pilot 1 \  
  --num_rounds_pilot 100 \  
  --num_rounds_actual 100 \  
  --lr_config_path 'lr_poly.json' \  
  --momentum 0.9 \  
  --gpu_index 0 \  
  --num_SGD_training 5 \  
  --batch_size_training 128 \  
  --num_SGD_grad_cal 5 \  
  --batch_size_grad_cal 128 \  
  --prox_alpha 1.0 \  
  --moon_mu 1.0 \  
  --moon_tau 1.0 \  
  --kl_coefficient 0.5 \  
  --acg_beta 0.1 \  
  --acg_lambda 0.5 \  
  --num_round_grad_cal 1 \  
  --similarity "two_norm" \  
  --similarity_scale 10.0
```

How hyperparameters were chosen: We selected all hyperparameters such that the training within each session converges by its final round. This ensures a fair comparison across different algorithms and datasets.

Baseline variants: AG News uses the average and previous baselines. All other datasets use average, previous, and continuous baselines.

20 Clients Configuration

- num_sessions=6
- acg_beta=0.01, acg_lambda=0.85
- prox_alpha=1.0 for FedProx
- Algorithms:
 - All datasets: FedAvg, FedProx, SCAFFOLD, FedACG
 - TinyImageNet: MOON (moon_mu=1.0, moon_tau=1.0), FedProx, FedACG
- kl_coefficient = 1.0 for all datasets except AG News (0.5)
- similarity_scale = 10.0 for all datasets except AG News (800)

- Random seeds: 0, 1, 2 (TinyImageNet uses 100, 200, 300)

100 Clients Configuration

- num_sessions=7
- acg_beta=0.1, acg_lambda=0.5
- Algorithms:
 - All datasets: MOON (moon_mu=1.0, moon_tau=1.0), FedProx (prox_alpha=1.0), SCAFFOLD, FedACG
- kl_coefficient = 1.0 for all datasets except AG News (0.5)
- similarity_scale = 10.0 for image datasets; AG News uses 800
- Random seeds: 100, 200, 300

Training Rounds (all clients)

- MNIST, Fashion-MNIST: 50 pilot rounds, 50 actual rounds
- SVHN, TinyImageNet: 200 pilot rounds, 200 actual rounds
- CIFAR-10, CIFAR-100: 150 pilot rounds, 150 actual rounds
- AG News: 100 pilot rounds, 100 actual rounds

Shared Parameters Across All Experiments

- momentum=0.9
- num_SGD_training=5, batch_size_training=128
- num_SGD_grad_cal=5, batch_size_grad_cal=128
- num_round_grad_cal=1
- Learning rate scheduler: lr_config_path = 'lr_poly.json'

D.2 Compute Resources

All experiments were conducted on a high-performance node provided by our university’s Advanced Computing Center, equipped with two Intel Xeon Platinum 8480+ 56-core CPUs (3.8 GHz), eight NVIDIA H100 GPUs (80 GB each), and 1031 GB of RAM. Each SLURM job was allocated one H100 GPU and 14 CPU cores.

Table 15 presents a comprehensive overview of average CPU time and maximum memory usage for our experiments with 20 clients. The average is taken over three random seeds.

Table 15: Average CPU time and average maximum memory usage across three random seeds for our experiments with 20 clients.

Dataset	Cross	Alpha	Method	CPU Time	Max Mem
MNIST	0.2	0.3	FedAvg	00:26:28	1.07G
MNIST	0.2	0.3	FedProx	00:26:33	1.11G
MNIST	0.2	0.3	SCAFFOLD	00:26:19	1.06G
MNIST	0.2	0.3	FedACG	00:26:18	1.10G
MNIST	0.2	0.7	FedAvg	00:25:51	1.06G
MNIST	0.2	0.7	FedProx	00:26:00	1.11G
MNIST	0.2	0.7	SCAFFOLD	00:25:45	1.05G
MNIST	0.2	0.7	FedACG	00:26:09	1.11G

Continued on next page

Dataset	Cross Vals	Alpha Vals	Method	CPU Time	Max Mem
MNIST	0.0	0.3	FedAvg	00:26:04	1.05G
MNIST	0.0	0.3	FedProx	00:26:13	1.12G
MNIST	0.0	0.3	SCAFFOLD	00:25:49	1.06G
MNIST	0.0	0.3	FedACG	00:25:53	1.10G
MNIST	0.0	0.7	FedAvg	00:26:08	1.06G
MNIST	0.0	0.7	FedProx	00:17:36	1.07G
MNIST	0.0	0.7	SCAFFOLD	00:17:29	1.03G
MNIST	0.0	0.7	FedACG	00:18:04	1.07G
FMNIST	0.2	0.3	FedAvg	00:25:52	1.10G
FMNIST	0.2	0.3	FedProx	00:26:09	1.14G
FMNIST	0.2	0.3	SCAFFOLD	00:25:58	1.07G
FMNIST	0.2	0.3	FedACG	00:26:18	1.13G
FMNIST	0.2	0.7	FedAvg	00:25:42	1.07G
FMNIST	0.2	0.7	FedProx	00:26:24	1.09G
FMNIST	0.2	0.7	SCAFFOLD	00:26:22	1.06G
FMNIST	0.2	0.7	FedACG	00:25:55	1.10G
FMNIST	0.0	0.3	FedAvg	00:25:50	1.08G
FMNIST	0.0	0.3	FedProx	00:26:28	1.10G
FMNIST	0.0	0.3	SCAFFOLD	00:26:10	1.06G
FMNIST	0.0	0.3	FedACG	00:26:25	1.11G
FMNIST	0.0	0.7	FedAvg	00:25:53	1.07G
FMNIST	0.0	0.7	FedProx	00:26:22	1.10G
FMNIST	0.0	0.7	SCAFFOLD	00:25:38	1.07G
FMNIST	0.0	0.7	FedACG	00:26:21	1.11G
SVHN	0.2	0.3	FedAvg	03:58:13	2.70G
SVHN	0.2	0.3	FedProx	04:14:29	2.74G
SVHN	0.2	0.3	SCAFFOLD	04:11:40	2.59G
SVHN	0.2	0.3	FedACG	04:16:08	2.46G
SVHN	0.2	0.7	FedAvg	04:01:22	2.69G
SVHN	0.2	0.7	FedProx	04:07:41	2.72G
SVHN	0.2	0.7	SCAFFOLD	04:01:41	2.57G
SVHN	0.2	0.7	FedACG	04:14:45	2.46G
SVHN	0.0	0.3	FedAvg	03:53:31	2.69G
SVHN	0.0	0.3	FedProx	04:03:16	2.72G
SVHN	0.0	0.3	SCAFFOLD	03:58:43	2.56G
SVHN	0.0	0.3	FedACG	04:04:32	2.42G
SVHN	0.0	0.7	FedAvg	03:57:38	2.67G
SVHN	0.0	0.7	FedProx	04:10:49	2.73G
SVHN	0.0	0.7	SCAFFOLD	04:00:49	2.57G
SVHN	0.0	0.7	FedACG	04:04:58	2.42G
CIFAR-10	0.2	0.3	FedAvg	04:48:29	13.67G
CIFAR-10	0.2	0.3	FedProx	05:22:40	13.74G
CIFAR-10	0.2	0.3	SCAFFOLD	06:30:16	14.68G
CIFAR-10	0.2	0.3	FedACG	05:51:08	13.33G
CIFAR-10	0.2	0.7	FedAvg	04:55:07	13.62G
CIFAR-10	0.2	0.7	FedProx	05:27:18	13.69G
CIFAR-10	0.2	0.7	SCAFFOLD	06:30:14	14.54G
CIFAR-10	0.2	0.7	FedACG	05:50:24	13.34G
CIFAR-10	0.0	0.3	FedAvg	04:55:51	13.65G
CIFAR-10	0.0	0.3	FedProx	05:31:49	13.72G

Continued on next page

Dataset	Cross Vals	Alpha Vals	Method	CPU Time	Max Mem
CIFAR-10	0.0	0.3	SCAFFOLD	06:33:56	14.55G
CIFAR-10	0.0	0.3	FedACG	05:51:33	13.35G
CIFAR-10	0.0	0.7	FedAvg	04:59:05	13.64G
CIFAR-10	0.0	0.7	FedProx	05:18:14	13.72G
CIFAR-10	0.0	0.7	SCAFFOLD	06:30:40	14.67G
CIFAR-10	0.0	0.7	FedACG	05:40:13	13.38G
CIFAR-100	0.2	0.3	FedAvg	05:07:17	13.66G
CIFAR-100	0.2	0.3	FedProx	05:27:38	13.78G
CIFAR-100	0.2	0.3	SCAFFOLD	06:34:27	14.61G
CIFAR-100	0.2	0.3	FedACG	05:45:00	13.22G
CIFAR-100	0.2	0.7	FedAvg	05:04:29	13.73G
CIFAR-100	0.2	0.7	FedProx	05:29:20	13.78G
CIFAR-100	0.2	0.7	SCAFFOLD	06:29:29	14.65G
CIFAR-100	0.2	0.7	FedACG	05:45:25	13.26G
CIFAR-100	0.0	0.3	FedAvg	04:53:37	13.71G
CIFAR-100	0.0	0.3	FedProx	05:25:04	13.82G
CIFAR-100	0.0	0.3	SCAFFOLD	06:30:22	14.56G
CIFAR-100	0.0	0.3	FedACG	05:43:58	13.24G
CIFAR-100	0.0	0.7	FedAvg	04:55:26	13.71G
CIFAR-100	0.0	0.7	FedProx	05:14:38	13.76G
CIFAR-100	0.0	0.7	SCAFFOLD	06:21:14	14.69G
CIFAR-100	0.0	0.7	FedACG	05:38:40	13.25G
TinyImageNet	0.2	0.3	MOON	18:39:30	26.12G
TinyImageNet	0.2	0.3	FedProx	16:22:46	25.01G
TinyImageNet	0.2	0.3	FedACG	17:02:45	23.38G
TinyImageNet	0.2	0.7	MOON	18:08:26	26.20G
TinyImageNet	0.2	0.7	FedProx	15:49:21	25.03G
TinyImageNet	0.2	0.7	FedACG	16:46:22	23.43G
TinyImageNet	0.0	0.3	MOON	18:09:04	26.17G
TinyImageNet	0.0	0.3	FedProx	15:22:17	25.12G
TinyImageNet	0.0	0.3	FedACG	16:31:42	23.34G
TinyImageNet	0.0	0.7	MOON	17:56:09	26.09G
TinyImageNet	0.0	0.7	FedProx	15:59:06	25.02G
TinyImageNet	0.0	0.7	FedACG	16:40:21	23.27G
AG News	0.8	0.3	FedAvg	01:04:40	9.97G
AG News	0.8	0.3	FedProx	01:05:43	10.02G
AG News	0.8	0.3	SCAFFOLD	02:29:40	8.61G
AG News	0.8	0.3	FedACG	01:19:28	8.62G
AG News	0.8	0.7	FedAvg	01:03:21	9.96G
AG News	0.8	0.7	FedProx	01:05:03	9.99G
AG News	0.8	0.7	SCAFFOLD	02:29:45	8.62G
AG News	0.8	0.7	FedACG	01:16:25	8.62G
AG News	0.0	0.3	FedAvg	01:02:22	9.98G
AG News	0.0	0.3	FedProx	01:03:02	9.99G
AG News	0.0	0.3	SCAFFOLD	02:27:12	8.59G
AG News	0.0	0.3	FedACG	01:15:39	8.67G
AG News	0.0	0.7	FedAvg	01:00:31	9.96G
AG News	0.0	0.7	FedProx	01:04:21	10.00G
AG News	0.0	0.7	SCAFFOLD	02:28:45	8.64G
AG News	0.0	0.7	FedACG	01:13:27	8.65G

Table 16 presents a comprehensive overview of average CPU time and average maximum memory usage for our experiments with 100 clients. The average is taken over three random seeds.

Table 16: Average CPU time and average maximum memory usage across three random seeds for our experiments with 100 clients.

Dataset	Cross	Alpha	Method	CPU Time	Max Mem
MNIST	0.2	0.3	MOON	00:59:59	1.29G
MNIST	0.2	0.3	FedProx	00:57:34	1.17G
MNIST	0.2	0.3	SCAFFOLD	00:56:08	1.11G
MNIST	0.2	0.3	FedACG	00:57:24	1.16G
MNIST	0.2	0.7	MOON	00:59:29	1.29G
MNIST	0.2	0.7	FedProx	00:57:02	1.17G
MNIST	0.2	0.7	SCAFFOLD	00:55:34	1.13G
MNIST	0.2	0.7	FedACG	00:56:42	1.15G
MNIST	0.0	0.3	MOON	00:59:09	1.28G
MNIST	0.0	0.3	FedProx	00:58:24	1.15G
MNIST	0.0	0.3	SCAFFOLD	00:56:19	1.13G
MNIST	0.0	0.3	FedACG	00:57:24	1.14G
MNIST	0.0	0.7	MOON	01:00:03	1.27G
MNIST	0.0	0.7	FedProx	00:58:13	1.16G
MNIST	0.0	0.7	SCAFFOLD	00:55:47	1.12G
MNIST	0.0	0.7	FedACG	00:57:15	1.17G
FMNIST	0.2	0.3	MOON	00:59:49	1.27G
FMNIST	0.2	0.3	FedProx	00:57:43	1.15G
FMNIST	0.2	0.3	SCAFFOLD	00:55:53	1.13G
FMNIST	0.2	0.3	FedACG	00:57:33	1.16G
FMNIST	0.2	0.7	MOON	00:59:47	1.29G
FMNIST	0.2	0.7	FedProx	00:57:40	1.16G
FMNIST	0.2	0.7	SCAFFOLD	00:56:19	1.11G
FMNIST	0.2	0.7	FedACG	00:57:41	1.16G
FMNIST	0.0	0.3	MOON	00:59:55	1.28G
FMNIST	0.0	0.3	FedProx	00:56:43	1.17G
FMNIST	0.0	0.3	SCAFFOLD	00:56:31	1.13G
FMNIST	0.0	0.3	FedACG	00:57:57	1.17G
FMNIST	0.0	0.7	MOON	00:59:52	1.27G
FMNIST	0.0	0.7	FedProx	00:58:14	1.16G
FMNIST	0.0	0.7	SCAFFOLD	00:56:14	1.12G
FMNIST	0.0	0.7	FedACG	00:57:09	1.15G
SVHN	0.2	0.3	MOON	11:38:02	6.44G
SVHN	0.2	0.3	FedProx	10:38:06	5.99G
SVHN	0.2	0.3	SCAFFOLD	10:29:37	5.85G
SVHN	0.2	0.3	FedACG	10:55:30	5.17G
SVHN	0.2	0.7	MOON	12:11:57	6.42G
SVHN	0.2	0.7	FedProx	11:14:06	6.09G
SVHN	0.2	0.7	SCAFFOLD	11:04:21	5.84G
SVHN	0.2	0.7	FedACG	10:56:34	5.17G
SVHN	0.0	0.3	MOON	11:50:13	6.48G
SVHN	0.0	0.3	FedProx	10:22:12	6.06G
SVHN	0.0	0.3	SCAFFOLD	10:14:38	5.96G
SVHN	0.0	0.3	FedACG	10:51:27	5.23G
SVHN	0.0	0.7	MOON	11:32:17	6.47G

Continued on next page

Dataset	Cross Vals	Alpha Vals	Method	CPU Time	Max Mem
SVHN	0.0	0.7	FedProx	11:03:23	6.09G
SVHN	0.0	0.7	SCAFFOLD	10:50:04	5.77G
SVHN	0.0	0.7	FedACG	10:36:18	5.19G
CIFAR-10	0.2	0.3	MOON	16:52:19	61.25G
CIFAR-10	0.2	0.3	FedProx	12:59:18	57.32G
CIFAR-10	0.2	0.3	SCAFFOLD	20:22:25	56.64G
CIFAR-10	0.2	0.3	FedACG	14:38:38	53.22G
CIFAR-10	0.2	0.7	MOON	17:31:36	61.08G
CIFAR-10	0.2	0.7	FedProx	13:19:24	57.28G
CIFAR-10	0.2	0.7	SCAFFOLD	20:15:41	56.52G
CIFAR-10	0.2	0.7	FedACG	14:25:16	53.29G
CIFAR-10	0.0	0.3	MOON	17:20:51	61.31G
CIFAR-10	0.0	0.3	FedProx	13:24:55	57.27G
CIFAR-10	0.0	0.3	SCAFFOLD	20:25:56	56.51G
CIFAR-10	0.0	0.3	FedACG	14:48:45	53.14G
CIFAR-10	0.0	0.7	MOON	17:26:10	61.26G
CIFAR-10	0.0	0.7	FedProx	13:23:31	57.17G
CIFAR-10	0.0	0.7	SCAFFOLD	20:03:12	56.40G
CIFAR-10	0.0	0.7	FedACG	14:50:02	53.19G
CIFAR-100	0.2	0.3	MOON	19:23:54	62.38G
CIFAR-100	0.2	0.3	FedProx	14:53:36	57.47G
CIFAR-100	0.2	0.3	SCAFFOLD	21:45:50	58.21G
CIFAR-100	0.2	0.3	FedACG	16:31:56	54.33G
CIFAR-100	0.2	0.7	MOON	19:05:52	62.30G
CIFAR-100	0.2	0.7	FedProx	14:58:14	57.43G
CIFAR-100	0.2	0.7	SCAFFOLD	21:39:22	58.15G
CIFAR-100	0.2	0.7	FedACG	16:18:23	54.22G
CIFAR-100	0.0	0.3	MOON	17:36:12	62.01G
CIFAR-100	0.0	0.3	FedProx	13:27:23	57.11G
CIFAR-100	0.0	0.3	SCAFFOLD	20:51:50	58.11G
CIFAR-100	0.0	0.3	FedACG	15:04:23	54.19G
CIFAR-100	0.0	0.7	MOON	17:43:03	62.00G
CIFAR-100	0.0	0.7	FedProx	13:26:15	57.19G
CIFAR-100	0.0	0.7	SCAFFOLD	20:09:42	58.26G
CIFAR-100	0.0	0.7	FedACG	14:50:34	54.36G
AG News	0.8	0.3	MOON	07:28:40	39.48G
AG News	0.8	0.3	FedProx	05:05:26	42.81G
AG News	0.8	0.3	SCAFFOLD	10:45:28	31.41G
AG News	0.8	0.3	FedACG	06:12:14	35.95G
AG News	0.8	0.7	MOON	07:26:40	39.39G
AG News	0.8	0.7	FedProx	05:14:55	42.77G
AG News	0.8	0.7	SCAFFOLD	11:04:57	31.39G
AG News	0.8	0.7	FedACG	06:02:33	35.95G
AG News	0.0	0.3	MOON	07:28:01	39.42G
AG News	0.0	0.3	FedProx	04:59:05	42.79G
AG News	0.0	0.3	SCAFFOLD	11:25:17	33.66G
AG News	0.0	0.3	FedACG	05:49:40	35.98G
AG News	0.0	0.7	MOON	07:29:04	39.55G
AG News	0.0	0.7	FedProx	05:11:57	42.84G
AG News	0.0	0.7	SCAFFOLD	10:57:00	31.42G

Continued on next page

Dataset	Cross Vals	Alpha Vals	Method	CPU Time	Max Mem
AG News	0.0	0.7	FedACG	05:51:58	36.01G
Tinyimagenet	0.2	0.3	MOON	71:04:06	107.02G
Tinyimagenet	0.2	0.3	FedProx	60:05:53	104.66G
Tinyimagenet	0.2	0.3	SCAFFOLD	72:56:11	95.09G
Tinyimagenet	0.2	0.3	FedACG	63:35:32	92.64G
Tinyimagenet	0.2	0.7	MOON	77:32:22	106.88G
Tinyimagenet	0.2	0.7	FedProx	64:33:53	104.34G
Tinyimagenet	0.2	0.7	SCAFFOLD	79:16:25	94.82G
Tinyimagenet	0.2	0.7	FedACG	66:31:58	92.48G
Tinyimagenet	0.0	0.3	MOON	70:13:51	106.77G
Tinyimagenet	0.0	0.3	FedProx	58:26:32	104.38G
Tinyimagenet	0.0	0.3	SCAFFOLD	73:27:39	95.02G
Tinyimagenet	0.0	0.3	FedACG	61:50:21	92.33G
Tinyimagenet	0.0	0.7	MOON	69:09:45	106.72G
Tinyimagenet	0.0	0.7	FedProx	59:04:02	104.18G
Tinyimagenet	0.0	0.7	SCAFFOLD	71:57:32	95.24G
Tinyimagenet	0.0	0.7	FedACG	61:02:40	92.33G

E Proof of Theorem 1

Based on the local training rule and global weighted average aggregation rule, the different between two global models is

$$\mathbf{w}^{(g+1)} - \mathbf{w}^{(g)} = \sum_{k \in \mathcal{K}^{(g)}} \frac{D_k^{(g)}}{D^{(g)}} \nabla \bar{F}_k^{(g)} \quad (6)$$

where $\nabla \bar{F}_k^{(g)}$ is the accumulated gradient across $e_k^{(g)}$ local steps given by

$$\nabla \bar{F}_k^{(g)} = \left(\mathbf{w}_k^{(g), e_k^{(g)}} - \mathbf{w}^{(g)} \right) = -\eta^{(g)} \sum_{e=1}^{e_k^{(g)}} \sum_{d \in \mathcal{B}_k^{(g), e}} \frac{\nabla f(\mathbf{w}_k^{(g)}, d)}{B_k^{(g)}} \quad (7)$$

Taking the expectation of (7) and using the fact that mini-batch sampling is conducted uniformly at random without replacement, we have

$$\mathbb{E} \left[\nabla \bar{F}_k^{(g)} \right] = -\eta^{(g)} \sum_{e=1}^{e_k^{(g)}} \sum_{d \in \mathcal{D}_k^{(g)}} \frac{\nabla f(\mathbf{w}_k^{(g)}, d)}{D_k^{(g)}} \quad (8)$$

Using the β -smoothness of the global loss function (Assumption 1), we have

$$F^{(g)}(\mathbf{w}^{(g+1)}) \leq F^{(g)}(\mathbf{w}^{(g)}) + \nabla F^{(g)}(\mathbf{w}^{(g)})^\top (\mathbf{w}^{(g+1)} - \mathbf{w}^{(g)}) + \frac{\beta}{2} \|\mathbf{w}^{(g+1)} - \mathbf{w}^{(g)}\|^2. \quad (9)$$

Plugging (6) and (7) into (9) and taking the expectation give

$$\begin{aligned} & \mathbb{E}_g \left[F^{(g)}(\mathbf{w}^{(g+1)}) \right] \\ & \leq F^{(g)}(\mathbf{w}^{(g)}) - \eta^{(g)} \nabla F^{(g)}(\mathbf{w}^{(g)})^\top \mathbb{E}_g \left[\sum_{k \in \mathcal{K}^{(g)}} \frac{D_k^{(g)}}{D^{(g)}} \sum_{e=1}^{e_k^{(g)}} \sum_{d \in \mathcal{D}_k^{(g), e}} \frac{\nabla f(\mathbf{w}_k^{(g), e-1}, d)}{D_k^{(g)}} \right] \\ & \quad + \frac{\beta}{2} \mathbb{E}_g \left[\left\| \eta^{(g)} \sum_{k \in \mathcal{K}^{(g)}} \frac{D_k^{(g)}}{D^{(g)}} \sum_{e=1}^{e_k^{(g)}} \sum_{d \in \mathcal{B}_k^{(g), e}} \frac{\nabla f(\mathbf{w}_k^{(g), e-1}, d)}{B_k^{(g)}} \right\|^2 \right] \end{aligned} \quad (10)$$

Using the fact that for any two real-valued vectors \mathbf{a} and \mathbf{b} with the same length, we have: $2\mathbf{a}^\top \mathbf{b} = \|\mathbf{a}\|^2 + \|\mathbf{b}\|^2 - \|\mathbf{a} - \mathbf{b}\|^2$, we further obtain

$$\begin{aligned} & \mathbb{E}_g \left[F^{(g)}(\mathbf{w}^{(g+1)}) \right] \leq F^{(g)}(\mathbf{w}^{(g)}) - \frac{\eta^{(g)}}{2} \sum_{k \in \mathcal{K}^{(g)}} \frac{D_k^{(g)}}{D^{(g)}} \mathbb{E}_g \left[\left\| \nabla F^{(g)}(\mathbf{w}^{(g)}) \right\|^2 \right. \\ & \quad + \left\| \sum_{k \in \mathcal{K}^{(g)}} \frac{D_k^{(g)}}{D^{(g)}} \sum_{e=1}^{e_k^{(g)}} \sum_{d \in \mathcal{D}_k^{(g), e}} \frac{\nabla f(\mathbf{w}_k^{(g), e-1}, d)}{D_k^{(g)}} \right\|^2 \\ & \quad + \left. \left\| \nabla F^{(g)}(\mathbf{w}^{(g)}) - \sum_{k \in \mathcal{K}^{(g)}} \frac{D_k^{(g)}}{D^{(g)}} \sum_{e=1}^{e_k^{(g)}} \sum_{d \in \mathcal{D}_k^{(g), e}} \frac{\nabla f(\mathbf{w}_k^{(g), e-1}, d)}{D_k^{(g)}} \right\|^2 \right] \\ & \quad + \frac{\beta(\eta^{(g)})^2}{2} \underbrace{\mathbb{E}_g \left[\left\| \sum_{k \in \mathcal{K}^{(g)}} \frac{D_k^{(g)}}{D^{(g)}} \sum_{e=1}^{e_k^{(g)}} \sum_{d \in \mathcal{B}_k^{(g), e}} \frac{\nabla f(\mathbf{w}_k^{(g), e-1}, d)}{B_k^{(g)}} \right\|^2 \right]}_{(a)} \end{aligned} \quad (11)$$

We first bound term (a) as follows.

$$\begin{aligned}
& \mathbb{E}_g \left[\left\| \sum_{k \in \mathcal{K}^{(g)}} \frac{D_k^{(g)}}{D^{(g)}} \sum_{e=1}^{e_k^{(g)}} \sum_{d \in \mathcal{B}_k^{(g),e}} \frac{\nabla f(\mathbf{w}_k^{(g),e-1}, d)}{B_k^{(g)}} \right\|^2 \right] \\
&= \mathbb{E}_g \left[\left\| \sum_{k \in \mathcal{K}^{(g)}} \frac{D_k^{(g)}}{D^{(g)}} \sum_{e=1}^{e_k^{(g)}} \left(\sum_{d \in \mathcal{B}_k^{(g),e}} \frac{\nabla f(\mathbf{w}_k^{(g),e-1}, d)}{B_k^{(g)}} - \sum_{d \in \mathcal{D}_k^{(g)}} \frac{\nabla f(\mathbf{w}_k^{(g),e-1}, d)}{D_k^{(g)}} \right) \right. \right. \\
&\quad \left. \left. + \sum_{d \in \mathcal{D}_k^{(g)}} \frac{\nabla f(\mathbf{w}_k^{(g),e-1}, d)}{D_k^{(g)}} \right) \right\|^2 \right] \\
&\stackrel{(i)}{\leq} 2 \mathbb{E}_g \left[\left\| \sum_{k \in \mathcal{K}^{(g)}} \frac{D_k^{(g)}}{D^{(g)}} \sum_{e=1}^{e_k^{(g)}} \left(\sum_{d \in \mathcal{B}_k^{(g),e}} \frac{\nabla f(\mathbf{w}_k^{(g),e-1}, d)}{B_k^{(g)}} - \sum_{d \in \mathcal{D}_k^{(g)}} \frac{\nabla f(\mathbf{w}_k^{(g),e-1}, d)}{D_k^{(g)}} \right) \right\|^2 \right] \\
&\quad + 2 \left\| \sum_{k \in \mathcal{K}^{(g)}} \frac{D_k^{(g)}}{D^{(g)}} \sum_{e=1}^{e_k^{(g)}} \sum_{d \in \mathcal{D}_k^{(g)}} \frac{\nabla f(\mathbf{w}_k^{(g),e-1}, d)}{D_k^{(g)}} \right\|^2 \\
&\stackrel{(ii)}{\leq} 2 \sum_{k \in \mathcal{K}^{(g)}} \frac{D_k^{(g)}}{D^{(g)}} \mathbb{E}_g \left[\left\| \sum_{d \in \mathcal{B}_k^{(g),e}} \frac{\nabla f(\mathbf{w}_k^{(g),e-1}, d)}{B_k^{(g)}} - \sum_{d \in \mathcal{D}_k^{(g)}} \frac{\nabla f(\mathbf{w}_k^{(g),e-1}, d)}{D_k^{(g)}} \right\|^2 \right] \\
&\quad + 2 \left\| \sum_{k \in \mathcal{K}^{(g)}} \frac{D_k^{(g)}}{D^{(g)}} \sum_{e=1}^{e_k^{(g)}} \sum_{d \in \mathcal{D}_k^{(g)}} \frac{\nabla f(\mathbf{w}_k^{(g),e-1}, d)}{D_k^{(g)}} \right\|^2 \\
&\stackrel{(iii)}{\leq} 2 \sum_{k \in \mathcal{K}^{(g)}} \frac{D_k^{(g)}}{D^{(g)}} \sum_{e=1}^{e_k^{(g)}} \left(1 - \frac{B_k^{(g)}}{D_k^{(g)}} \right) \frac{(\sigma_k^{(g),e-1})^2}{B_k^{(g)}} \\
&\quad + 2 \left\| \sum_{k \in \mathcal{K}^{(g)}} \frac{D_k^{(g)}}{D^{(g)}} \sum_{e=1}^{e_k^{(g)}} \sum_{d \in \mathcal{D}_k^{(g)}} \frac{\nabla f(\mathbf{w}_k^{(g),e-1}, d)}{D_k^{(g)}} \right\|^2. \tag{12}
\end{aligned}$$

where (i) we have used the Cauchy-Schwarz inequality $\|\mathbf{a} + \mathbf{b}\|^2 \leq 2\|\mathbf{a}\|^2 + 2\|\mathbf{b}\|^2$, (ii) we used the convex property of 2-norm, (iii) we used Eq (3.5) in chapter 3 of [51] and the definition of variance of the gradients $(\sigma_k^{(g),e-1})^2$ evaluated at the particular local step $e - 1$ for the parameter realization $\mathbf{w}_k^{(g),e-1}$. Expanding $(\sigma_k^{(g),e-1})^2$ yields

$$\begin{aligned}
& (\sigma_k^{(g),e-1})^2 \\
&= \frac{\sum_{d \in \mathcal{D}_k^{(g)}} \left\| \nabla f(\mathbf{w}_k^{(g),e-1}, d) - \frac{\sum_{d' \in \mathcal{D}_k^{(g)}} \nabla f(\mathbf{w}_k^{(g),e-1}, d')}{D_k^{(g)}} \right\|^2}{D_k^{(g)} - 1} \\
&= \frac{\sum_{d \in \mathcal{D}_k^{(g)}} \left(\frac{1}{D_k^{(g)}} \right)^2 \left\| D_k^{(g)} \nabla f(\mathbf{w}_k^{(g),e-1}, d) - \sum_{d' \in \mathcal{D}_k^{(g)}} \nabla f(\mathbf{w}_k^{(g),e-1}, d') \right\|^2}{D_k^{(g)} - 1} \\
&\stackrel{(i)}{\leq} \frac{\sum_{d \in \mathcal{D}_k^{(g)}} \frac{(D_k^{(g)} - 1)}{(D_k^{(g)})^2} \sum_{d' \in \mathcal{D}_k^{(g)}} \left\| \nabla f(\mathbf{w}_k^{(g),e-1}, d) - \nabla f(\mathbf{w}_k^{(g),e-1}, d') \right\|^2}{D_k^{(g)} - 1} \\
&\leq \frac{1}{(D_k^{(g)})^2} (\Theta^{(g)})^2 \sum_{d \in \mathcal{D}_k^{(g)}} \sum_{d' \in \mathcal{D}_k^{(g)}} \|d - d'\|^2
\end{aligned}$$

$$\begin{aligned}
&\leq \frac{1}{(D_k^{(g)})^2} (\Theta^{(g)})^2 \sum_{d \in \mathcal{D}_k^{(g)}} \sum_{d' \in \mathcal{D}_k^{(g)}} \|d - d'\|^2 \\
&\leq \frac{(\Theta^{(g)})^2}{(D_k^{(g)})^2} \sum_{d \in \mathcal{D}_k^{(g)}} \sum_{d' \in \mathcal{D}_k^{(g)}} \|d - \lambda_k^{(g)} - d' + \lambda_k^{(g)}\|^2 \\
&\leq \frac{(\Theta^{(g)})^2}{(D_k^{(g)})^2} \sum_{d \in \mathcal{D}_k^{(g)}} \sum_{d' \in \mathcal{D}_k^{(g)}} \left(\|d - \lambda_k^{(g)}\|^2 + \|d' - \lambda_k^{(g)}\|^2 + 2(d - \lambda_k^{(g)})^\top (d' - \lambda_k^{(g)}) \right) \\
&\stackrel{(ii)}{\leq} \frac{(\Theta^{(g)})^2}{(D_k^{(g)})^2} \left(D_k^{(g)} \sum_{d \in \mathcal{D}_k^{(g)}} \|d - \lambda_k^{(g)}\|^2 + D_k^{(g)} \sum_{d' \in \mathcal{D}_k^{(g)}} \|d' - \lambda_k^{(g)}\|^2 \right) \\
&\leq \frac{2(\Theta^{(g)})^2}{D_k^{(g)}} (\tilde{\sigma}_k^{(g)})^2. \tag{13}
\end{aligned}$$

where d denotes the feature vector of data point d , and $\lambda_k^{(g)}$ and $(\tilde{\sigma}_k^{(g)})^2$ denote the mean and sample variance of data points in $\mathcal{D}_k^{(g)}$, which are gradient independent. Also, in (i) of (13), we used the Cauchy-Schwarz inequality, and in (ii), we used the fact that $\sum_{d \in \mathcal{D}_k^{(g)}} (d - \lambda_k^{(g)}) = 0$. Plugging (13) into (12) gives

$$\begin{aligned}
&\mathbb{E}_g \left[\left\| \sum_{k \in \mathcal{K}^{(g)}} \frac{D_k^{(g)}}{D^{(g)}} \sum_{e=1}^{e_k^{(g)}} \sum_{d \in \mathcal{B}_k^{(g),e}} \frac{\nabla f(\mathbf{w}_k^{(g),e-1}, d)}{B_k^{(g),e}} \right\|^2 \right] \\
&\leq 4(\Theta^{(g)})^2 \sum_{k \in \mathcal{K}^{(g)}} \frac{D_k^{(g)}}{D^{(g)}} (\tilde{\sigma}_k^{(g)})^2 \sum_{e=1}^{e_k^{(g)}} \left(1 - \frac{B_k^{(g)}}{D_k^{(g)}} \right) \frac{1}{B_k^{(g)}} \\
&\quad + 2 \left\| \sum_{k \in \mathcal{K}^{(g)}} \frac{D_k^{(g)}}{D^{(g)}} \sum_{e=1}^{e_k^{(g)}} \sum_{d \in \mathcal{D}_k^{(g)}} \frac{\nabla f(\mathbf{w}_k^{(g),e-1}, d)}{D_k^{(g)}} \right\|^2.
\end{aligned}$$

Using this, (12) becomes

$$\begin{aligned}
\mathbb{E}_g [F^{(g)}(\mathbf{w}^{(g+1)})] &\leq F^{(g)}(\mathbf{w}^{(g)}) - \frac{\eta^{(g)}}{2} \sum_{k \in \mathcal{K}^{(g)}} \frac{D_k^{(g)}}{D^{(g)}} \mathbb{E}_g \left[\left\| \nabla F^{(g)}(\mathbf{w}^{(g)}) \right\|^2 \right] \\
&\quad + \left\| \sum_{k \in \mathcal{K}^{(g)}} \frac{D_k^{(g)}}{D^{(g)}} \sum_{e=1}^{e_k^{(g)}} \sum_{d \in \mathcal{D}_k^{(g),e}} \frac{\nabla f(\mathbf{w}_k^{(g),e-1}, d)}{D_k^{(g)}} \right\|^2 \\
&\quad + \left\| \nabla F^{(g)}(\mathbf{w}^{(g)}) - \sum_{k \in \mathcal{K}^{(g)}} \frac{D_k^{(g)}}{D^{(g)}} \sum_{e=1}^{e_k^{(g)}} \sum_{d \in \mathcal{D}_k^{(g),e}} \frac{\nabla f(\mathbf{w}_k^{(g),e-1}, d)}{D_k^{(g)}} \right\|^2 \\
&\quad + 2\beta(\eta^{(g)})^2 (\Theta^{(g)})^2 \sum_{k \in \mathcal{K}^{(g)}} \frac{D_k^{(g)}}{D^{(g)}} (\tilde{\sigma}_k^{(g)})^2 \sum_{e=1}^{e_k^{(g)}} \left(1 - \frac{B_k^{(g)}}{D_k^{(g)}} \right) \frac{1}{B_k^{(g)}} \\
&\quad + \beta(\eta^{(g)})^2 \left\| \sum_{k \in \mathcal{K}^{(g)}} \frac{D_k^{(g)}}{D^{(g)}} \sum_{e=1}^{e_k^{(g)}} \sum_{d \in \mathcal{D}_k^{(g)}} \frac{\nabla f(\mathbf{w}_k^{(g),e-1}, d)}{D_k^{(g)}} \right\|^2. \tag{14}
\end{aligned}$$

Rearranging the terms, we have

$$\mathbb{E}_g [F^{(g)}(\mathbf{w}^{(g+1)})]$$

$$\begin{aligned}
&\leq F^{(g)}(\mathbf{w}^{(g)}) - \frac{\eta^{(g)}}{2} \sum_{k \in \mathcal{K}^{(g)}} \frac{D_k^{(g)}}{D^{(g)}} \mathbb{E}_g [\|\nabla F^{(g)}(\mathbf{w}^{(g)})\|^2] \\
&\quad + \left(\beta(\eta^{(g)})^2 - \frac{\eta^{(g)}}{2} \right) \sum_{k \in \mathcal{K}^{(g)}} \frac{D_k^{(g)}}{D^{(g)}} \mathbb{E}_g \left[\left\| \sum_{e=1}^{e_k^{(g)}} \sum_{d \in \mathcal{D}_k^{(g)}} \frac{\nabla f(\mathbf{w}_k^{(g),e-1}, d)}{D_k^{(g)}} \right\|^2 \right] \\
&\quad + \underbrace{\frac{\eta^{(g)}}{2} \sum_{k \in \mathcal{K}^{(g)}} \frac{D_k^{(g)}}{D^{(g)}} \mathbb{E}_g \left[\left\| \nabla F^{(g)}(\mathbf{w}^{(g)}) - \sum_{e=1}^{e_k^{(g)}} \sum_{d \in \mathcal{D}_k^{(g)}} \frac{\nabla f(\mathbf{w}_k^{(g),e-1}, d)}{D_k^{(g)}} \right\|^2 \right]}_{(b)} \\
&\quad + 2\beta(\Theta^{(g)})^2(\eta^{(g)})^2 \sum_{k \in \mathcal{K}^{(g)}} \frac{(\tilde{\sigma}_k^{(g)})^2}{D_k^{(g)}} \sum_{e=1}^{e_k^{(g)}} \left(1 - \frac{B_k^{(g)}}{D_k^{(g)}} \right) \frac{1}{B_k^{(g)}}. \tag{15}
\end{aligned}$$

Term (b) in (15) can be upper bounded as

$$\begin{aligned}
&\frac{\eta^{(g)}}{2} \sum_{k \in \mathcal{K}^{(g)}} \frac{D_k^{(g)}}{D^{(g)}} \mathbb{E}_g \left[\left\| \nabla F^{(g)}(\mathbf{w}^{(g)}) - \sum_{e=1}^{e_k^{(g)}} \sum_{d \in \mathcal{D}_k^{(g)}} \frac{\nabla f(\mathbf{w}_k^{(g),e-1}, d)}{D_k^{(g)}} \right\|^2 \right] \\
&= \frac{\eta^{(g)}}{2} \sum_{k \in \mathcal{K}^{(g)}} \frac{D_k^{(g)}}{D^{(g)}} \mathbb{E}_g \left[\left\| \nabla F^{(g)}(\mathbf{w}^{(g)}) - \frac{1}{e_k^{(g)}} \sum_{e=1}^{e_k^{(g)}} \sum_{d \in \mathcal{D}_k^{(g)}} \frac{\nabla f(\mathbf{w}_k^{(g),e-1}, d)}{D_k^{(g)}} \right. \right. \\
&\quad \left. \left. + \left(\frac{1}{e_k^{(g)}} - 1 \right) \sum_{e=1}^{e_k^{(g)}} \sum_{d \in \mathcal{D}_k^{(g)}} \frac{\nabla f(\mathbf{w}_k^{(g),e-1}, d)}{D_k^{(g)}} \right\|^2 \right] \\
&\leq \eta^{(g)} \sum_{k \in \mathcal{K}^{(g)}} \frac{D_k^{(g)}}{D^{(g)}} \mathbb{E}_g \left[\underbrace{\left\| \nabla F^{(g)}(\mathbf{w}^{(g)}) - \frac{1}{e_k^{(g)}} \sum_{e=1}^{e_k^{(g)}} \sum_{d \in \mathcal{D}_k^{(g)}} \nabla f(\mathbf{w}_k^{(g),e-1}, d) \right\|^2}_{(b1)} \right] \\
&\quad + \eta^{(g)} \left(\frac{1}{e_{\min}^{(g)}} - 1 \right)^2 \sum_{k \in \mathcal{K}^{(g)}} \frac{D_k^{(g)}}{D^{(g)}} \mathbb{E}_g \left[\left\| \sum_{e=1}^{e_k^{(g)}} \sum_{d \in \mathcal{D}_k^{(g)}} \nabla f(\mathbf{w}_k^{(g),e-1}, d) \right\|^2 \right]. \tag{16}
\end{aligned}$$

where $e_{\min}^{(g)} = \min_{k \in \mathcal{K}^{(g)}} e_k^{(g)}$ is the minimum number of local steps in the g -th round. Term (b1) in (16) can be upper bounded as

$$\begin{aligned}
&\mathbb{E}_g \left[\left\| \nabla F^{(g)}(\mathbf{w}^{(g)}) - \frac{1}{e_k^{(g)}} \sum_{e=1}^{e_k^{(g)}} \sum_{d \in \mathcal{D}_k^{(g)}} \frac{\nabla f(\mathbf{w}_k^{(g),e-1}, d)}{D_k^{(g)}} \right\|^2 \right] \\
&= \mathbb{E}_g \left[\left\| \nabla F^{(g)}(\mathbf{w}^{(g)}) - \frac{1}{e_k^{(g)}} \sum_{e=1}^{e_k^{(g)}} \nabla F_k^{(g)}(\mathbf{w}_k^{(g),e-1}) \right\|^2 \right] \\
&\leq \sum_{k \in \mathcal{K}^{(g)}} \frac{D_k^{(g)}}{D^{(g)}} \mathbb{E}_g \left[\left\| \nabla F_k^{(g)}(\mathbf{w}^{(g)}) - \frac{1}{e_k^{(g)}} \sum_{e=1}^{e_k^{(g)}} \nabla F_k^{(g)}(\mathbf{w}_k^{(g),e-1}) \right\|^2 \right] \\
&\leq \sum_{k \in \mathcal{K}^{(g)}} \frac{D_k^{(g)}}{D^{(g)} e_k^{(g)}} \sum_{e=1}^{e_k^{(g)}} \mathbb{E}_g \left[\left\| \nabla F_k^{(g)}(\mathbf{w}_k^{(g)}) - \nabla F_k^{(g)}(\mathbf{w}_k^{(g),e-1}) \right\|^2 \right]
\end{aligned}$$

$$\leq \sum_{k \in \mathcal{K}^{(g)}} \frac{D_k^{(g)}}{D^{(g)} e_k^{(g)}} \sum_{e=1}^{e_k^{(g)}} \beta^2 \mathbb{E}_g \left[\|\mathbf{w}^{(g)} - \mathbf{w}_k^{(g),e-1}\|^2 \right]. \quad (17)$$

Using the local update rule, $\mathbb{E}_g \|\mathbf{w}^{(g)} - \mathbf{w}_k^{(g),e-1}\|^2$ can be further upper bounded as

$$\begin{aligned} & \mathbb{E}_g \|\mathbf{w}^{(g)} - \mathbf{w}_k^{(g),e-1}\|^2 \\ &= (\eta^{(g)})^2 \mathbb{E}_g \left\| \sum_{e'=1}^{e-1} \sum_{d \in \mathcal{B}_k^{(g),e}} \frac{\nabla f(\mathbf{w}_k^{(g),e-1}, d)}{B_k^{(g)}} \right\|^2 \\ &= (\eta^{(g)})^2 \mathbb{E}_g \left\| \sum_{e'=1}^{e-1} \left(\sum_{d \in \mathcal{B}_k^{(g),e}} \frac{\nabla f(\mathbf{w}_k^{(g),e-1}, d)}{B_k^{(g)}} - \sum_{d \in \mathcal{D}_k^{(g)}} \frac{\nabla f(\mathbf{w}_k^{(g),e-1}, d)}{D_k^{(g)}} \right. \right. \\ & \quad \left. \left. + \sum_{d \in \mathcal{D}_k^{(g)}} \frac{\nabla f(\mathbf{w}_k^{(g),e-1}, d)}{D_k^{(g)}} \right) \right\|^2 \\ &\leq 2(\eta^{(g)})^2 \mathbb{E}_g \left\| \sum_{e'=1}^{e-1} \left(\sum_{d \in \mathcal{B}_k^{(g),e}} \frac{\nabla f(\mathbf{w}_k^{(g),e-1}, d)}{B_k^{(g)}} - \sum_{d \in \mathcal{D}_k^{(g)}} \frac{\nabla f(\mathbf{w}_k^{(g),e-1}, d)}{D_k^{(g)}} \right) \right\|^2 \\ & \quad + 2(\eta^{(g)})^2 \mathbb{E}_g \left\| \sum_{e'=1}^{e-1} \sum_{d \in \mathcal{D}_k^{(g)}} \frac{\nabla f(\mathbf{w}_k^{(g),e-1}, d)}{D_k^{(g)}} \right\|^2 \\ &\leq 2(\eta^{(g)})^2 \sum_{e'=1}^{e-1} \mathbb{E}_g \left\| \sum_{d \in \mathcal{B}_k^{(g),e}} \frac{\nabla f(\mathbf{w}_k^{(g),e-1}, d)}{B_k^{(g)}} - \sum_{d \in \mathcal{D}_k^{(g)}} \frac{\nabla f(\mathbf{w}_k^{(g),e-1}, d)}{D_k^{(g)}} \right\|^2 \\ & \quad + 2(\eta^{(g)})^2 \mathbb{E}_g \left\| \sum_{e'=1}^{e-1} \sum_{d \in \mathcal{D}_k^{(g)}} \frac{\nabla f(\mathbf{w}_k^{(g),e-1}, d)}{D_k^{(g)}} \right\|^2 \\ &\leq 4(\eta^{(g)})^2 \sum_{e'=1}^{e-1} \left(1 - \frac{B_k^{(g)}}{D_k^{(g)}} \right) \frac{(\Theta^{(g)})^2}{B_k^{(g)} D_k^{(g)}} (\tilde{\sigma}_k^{(g)})^2 \\ & \quad + 2(\eta^{(g)})^2 \mathbb{E}_g \left\| \sum_{e'=1}^{e-1} \sum_{d \in \mathcal{D}_k^{(g)}} \frac{\nabla f(\mathbf{w}_k^{(g),e-1}, d)}{D_k^{(g)}} \right\|^2. \quad (18) \end{aligned}$$

The last term in (18) can be further upper bounded

$$\begin{aligned} & 2(\eta^{(g)})^2 \mathbb{E}_g \left\| \sum_{e'=1}^{e-1} \sum_{d \in \mathcal{D}_k^{(g)}} \frac{\nabla f(\mathbf{w}_k^{(g),e'-1}, d)}{D_k^{(g)}} \right\|^2 \\ &\leq 2(\eta^{(g)})^2 (e-1) \sum_{e'=1}^{e-1} \mathbb{E}_g \left\| \sum_{d \in \mathcal{D}_k^{(g)}} \frac{\nabla f(\mathbf{w}_k^{(g),e'-1}, d)}{D_k^{(g)}} \right\|^2 \\ &\leq 2(\eta^{(g)})^2 (e-1) \sum_{e'=1}^{e-1} \mathbb{E}_g \left\| \nabla F_k^{(g)}(\mathbf{w}_k^{(g),e'-1}) - \nabla F_k^{(g)}(\mathbf{w}^{(g)}) + \nabla F_k^{(g)}(\mathbf{w}^{(g)}) \right\|^2 \\ &\leq 4(\eta^{(g)})^2 (e-1) \sum_{e'=1}^{e-1} \mathbb{E}_g \left\| \nabla F_k^{(g)}(\mathbf{w}_k^{(g),e'-1}) - \nabla F_k^{(g)}(\mathbf{w}^{(g)}) \right\|^2 \\ & \quad + 4(\eta^{(g)})^2 (e-1) \sum_{e'=1}^{e-1} \left\| \nabla F_k^{(g)}(\mathbf{w}^{(g)}) \right\|^2 \end{aligned}$$

$$\begin{aligned}
&\leq 4\beta^2(\eta^{(g)})^2(e-1) \sum_{e'=1}^{e-1} \mathbb{E}_g \left\| \mathbf{w}_k^{(g),e'-1} - \mathbf{w}^{(g)} \right\|^2 \\
&\quad + 4(\eta^{(g)})^2(e-1) \sum_{e'=1}^{e-1} \left\| \nabla F_k^{(g)}(\mathbf{w}^{(g)}) \right\|^2.
\end{aligned} \tag{19}$$

Combining (19) with (18) gives

$$\begin{aligned}
&\mathbb{E}_g \left\| \mathbf{w}^{(g)} - \mathbf{w}_k^{(g),e-1} \right\|^2 \\
&\leq 4(\eta^{(g)})^2 \sum_{e'=1}^{e-1} \left(1 - \frac{B_k^{(g)}}{D_k^{(g)}} \right) \frac{(\Theta^{(g)})^2}{B_k^{(g)} D_k^{(g)}} (\tilde{\sigma}_k^{(g)})^2 \\
&\quad + 4\beta^2(\eta^{(g)})^2(e-1) \sum_{e'=1}^{e-1} \mathbb{E}_g \left\| \mathbf{w}_k^{(g),e'-1} - \mathbf{w}^{(g)} \right\|^2 \\
&\quad + 4(\eta^{(g)})^2(e-1) \sum_{e'=1}^{e-1} \left\| \nabla F_k^{(g)}(\mathbf{w}^{(g)}) \right\|^2.
\end{aligned} \tag{20}$$

Taking the summation of both sides in (20) across local training steps

$$\begin{aligned}
&\sum_{e=1}^{e_k^{(g)}} \mathbb{E}_g \left\| \mathbf{w}^{(g)} - \mathbf{w}_k^{(g),e-1} \right\|^2 \\
&\leq 4(\eta^{(g)})^2 \sum_{e=1}^{e_k^{(g)}} \sum_{e'=1}^{e-1} \left(1 - \frac{B_k^{(g)}}{D_k^{(g)}} \right) \frac{(\Theta^{(g)})^2}{B_k^{(g)} D_k^{(g)}} (\tilde{\sigma}_k^{(g)})^2 \\
&\quad + 4\beta^2(\eta^{(g)})^2 \sum_{e=1}^{e_k^{(g)}} (e-1) \sum_{e'=1}^{e-1} \mathbb{E}_g \left\| \mathbf{w}_k^{(g),e'-1} - \mathbf{w}^{(g)} \right\|^2 \\
&\quad + 4(\eta^{(g)})^2 \sum_{e=1}^{e_k^{(g)}} (e-1) \sum_{e'=1}^{e-1} \left\| \nabla F_k^{(g)}(\mathbf{w}^{(g)}) \right\|^2.
\end{aligned}$$

After some simplification, we obtain

$$\begin{aligned}
&\sum_{e=1}^{e_k^{(g)}} \mathbb{E}_g \left\| \mathbf{w}^{(g)} - \mathbf{w}_k^{(g),e-1} \right\|^2 \\
&\leq 2(\eta^{(g)})^2 (e_k^{(g)} - 1) e_k^{(g)} \left(1 - \frac{B_k^{(g)}}{D_k^{(g)}} \right) \frac{(\Theta^{(g)})^2}{B_k^{(g)} D_k^{(g)}} (\tilde{\sigma}_k^{(g)})^2 \\
&\quad + 4\beta^2(\eta^{(g)})^2 e_k^{(g)} (e_k^{(g)} - 1) \sum_{e=1}^{e_k^{(g)}} \mathbb{E}_g \left\| \mathbf{w}^{(g)} - \mathbf{w}_k^{(g),e-1} \right\|^2 \\
&\quad + 4(\eta^{(g)})^2 e_k^{(g)} (e_k^{(g)} - 1) \sum_{e=1}^{e_k^{(g)}} \left\| \nabla F_k^{(g)}(\mathbf{w}^{(g)}) \right\|^2.
\end{aligned} \tag{21}$$

Assuming

$$\eta^{(g)} \leq \left(2\beta^2 \sqrt{e_k^{(g)} (e_k^{(g)} - 1)} \right)^{-1},$$

Performing some algebraic operations and combining the same terms on (21) gives

$$\sum_{e=1}^{e_k^{(g)}} \mathbb{E}_g \left\| \mathbf{w}^{(g)} - \mathbf{w}_k^{(g),e-1} \right\|^2$$

$$\begin{aligned}
&\leq \frac{2(\eta^{(g)})^2(e_k^{(g)} - 1)e_k^{(g)}}{1 - 4\beta^2(\eta^{(g)})^2e_k^{(g)}(e_k^{(g)} - 1)} \left(1 - \frac{B_k^{(g)}}{D_k^{(g)}}\right) \frac{(\Theta^{(g)})^2}{B_k^{(g)}D_k^{(g)}} (\tilde{\sigma}_k^{(g)})^2 \\
&\quad + \frac{4(\eta^{(g)})^2(e_k^{(g)}(e_k^{(g)} - 1))}{1 - 4\beta^2(\eta^{(g)})^2e_k^{(g)}(e_k^{(g)} - 1)} \sum_{e=1}^{e_k^{(g)}} \|\nabla F_k^{(g)}(\mathbf{w}^{(g)})\|^2. \tag{22}
\end{aligned}$$

Let $e_{\max}^{(g)} = \max_{k \in \mathcal{K}^{(g)}} e_k^{(g)}$ be the maximum number of local steps in the g -th round, plugging (22) in (17) gives

$$\begin{aligned}
&\mathbb{E}_g \|\nabla F^{(g)}(\mathbf{w}^{(g)}) - \frac{1}{e_k^{(g)}} \sum_{e=1}^{e_k^{(g)}} \sum_{d \in \mathcal{D}_k^{(g)}} \nabla f(\mathbf{w}_k^{(g),e-1}, d)\|^2 \\
&\leq 2(\eta^{(g)})^2\beta^2 \sum_{k \in \mathcal{K}^{(g)}} \frac{D_k^{(g)}}{D^{(g)}} \frac{e_k^{(g)} - 1}{1 - 4\beta^2(\eta^{(g)})^2e_k^{(g)}(e_k^{(g)} - 1)} \left(1 - \frac{B_k^{(g)}}{D_k^{(g)}}\right) \frac{(\Theta^{(g)})^2}{B_k^{(g)}D_k^{(g)}} (\tilde{\sigma}_k^{(g)})^2 \\
&\quad + \frac{4\beta^2(\eta^{(g)})^2(e_{\max}^{(g)}(e_{\max}^{(g)} - 1))}{1 - 4\beta^2(\eta^{(g)})^2e_{\max}^{(g)}(e_{\max}^{(g)} - 1)} \sum_{k \in \mathcal{K}^{(g)}} \frac{D_k^{(g)}}{D^{(g)}} \mathbb{E}_g \|\nabla F_k^{(g)}(\mathbf{w}^{(g)})\|^2 \\
&\stackrel{(i)}{\leq} 2(\eta^{(g)})^2\beta^2 \sum_{k \in \mathcal{K}^{(g)}} \frac{D_k^{(g)}}{D^{(g)}} \frac{e_k^{(g)} - 1}{1 - 4\beta^2(\eta^{(g)})^2e_k^{(g)}(e_k^{(g)} - 1)} \left(1 - \frac{B_k^{(g)}}{D_k^{(g)}}\right) \frac{(\Theta^{(g)})^2}{B_k^{(g)}D_k^{(g)}} (\tilde{\sigma}_k^{(g)})^2 \\
&\quad + \frac{4\beta^2(\eta^{(g)})^2(e_{\max}^{(g)}(e_{\max}^{(g)} - 1))}{1 - 4\beta^2(\eta^{(g)})^2e_{\max}^{(g)}(e_{\max}^{(g)} - 1)} \left(\zeta_1 \mathbb{E}_g \left\| \sum_{k \in \mathcal{K}^{(g)}} \frac{D_k^{(g)}}{D^{(g)}} \nabla F_k^{(g)}(\mathbf{w}^{(g)}) \right\|^2 + \zeta_2 \right) \\
&\leq 2(\eta^{(g)})^2\beta^2 \sum_{k \in \mathcal{K}^{(g)}} \frac{D_k^{(g)}}{D^{(g)}} \frac{e_k^{(g)} - 1}{1 - 4\beta^2(\eta^{(g)})^2e_k^{(g)}(e_k^{(g)} - 1)} \left(1 - \frac{B_k^{(g)}}{D_k^{(g)}}\right) \frac{(\Theta^{(g)})^2}{B_k^{(g)}D_k^{(g)}} (\tilde{\sigma}_k^{(g)})^2 \\
&\quad + \frac{4\beta^2(\eta^{(g)})^2(e_{\max}^{(g)})^2(e_{\max}^{(g)} - 1)}{1 - 4\beta^2(\eta^{(g)})^2e_{\max}^{(g)}(e_{\max}^{(g)} - 1)} \left(\zeta_1 \mathbb{E}_g \|\nabla F^{(g)}(\mathbf{w}^{(g)})\|^2 + \zeta_2 \right). \tag{23}
\end{aligned}$$

Plugging (23) into (15) gives

$$\begin{aligned}
\mathbb{E}_g [F^{(g)}(\mathbf{w}^{(g+1)})] &\leq F^{(g)}(\mathbf{w}^{(g)}) + 2\beta(\Theta^{(g)})^2(\eta^{(g)})^2 \sum_{k \in \mathcal{K}^{(g)}} \frac{(\tilde{\sigma}_k^{(g)})^2}{D_k^{(g)}} \sum_{e=1}^{e_k^{(g)}} \left(1 - \frac{B_k^{(g)}}{D_k^{(g)}}\right) \frac{1}{B_k^{(g)}} \\
&\quad + (\eta^{(g)})^3\beta^2 \sum_{k \in \mathcal{K}^{(g)}} \frac{D_k^{(g)}}{D^{(g)}} \frac{e_k^{(g)} - 1}{1 - 4\beta^2(\eta^{(g)})^2e_k^{(g)}(e_k^{(g)} - 1)} \left(1 - \frac{B_k^{(g)}}{D_k^{(g)}}\right) \frac{(\Theta^{(g)})^2}{B_k^{(g)}D_k^{(g)}} (\tilde{\sigma}_k^{(g)})^2 \\
&\quad + \underbrace{\left(\beta(\eta^{(g)})^2 - \frac{\eta^{(g)}}{2} + \eta^{(g)} \left(\frac{1}{e_{\min}^{(g)}} - 1 \right) \right) \sum_{k \in \mathcal{K}^{(g)}} \frac{D_k^{(g)}}{D^{(g)}} \mathbb{E}_g \left\| \sum_{e=1}^{e_k^{(g)}} \sum_{d \in \mathcal{D}_k^{(g)}} \frac{\nabla f(\mathbf{w}_k^{(g),e-1}, d)}{D_k^{(g)}} \right\|^2}_{(c)} \\
&\quad + \frac{2\beta^2(\eta^{(g)})^3(e_{\max}^{(g)})^2(e_{\max}^{(g)} - 1)}{1 - 4\beta^2(\eta^{(g)})^2e_{\max}^{(g)}(e_{\max}^{(g)} - 1)} \zeta_2 \\
&\quad + \frac{\eta^{(g)}}{2} \left(\frac{4\beta^2(\eta^{(g)})^2(e_{\max}^{(g)})^2(e_{\max}^{(g)} - 1)}{1 - 4\beta^2(\eta^{(g)})^2e_{\max}^{(g)}(e_{\max}^{(g)} - 1)} \zeta_1 - 1 \right) \left\| \nabla F^{(g)}(\mathbf{w}^{(g)}) \right\|^2. \tag{24}
\end{aligned}$$

To eliminate term (c) in (24), we need to make

$$\beta(\eta^{(g)})^2 - \frac{\eta^{(g)}}{2} + \eta^{(g)} \left(\frac{1}{e_{\min}^{(g)}} - 1 \right)^2 < 0, \tag{25}$$

we require

$$\eta^{(g)} < \left(\frac{1}{2} - \left(\frac{1}{e_{\min}^{(g)}} - 1 \right)^2 \right) \frac{1}{\beta}. \quad (26)$$

Also, we aim to make

$$\frac{4\beta^2(\eta^{(g)})^2(e_{\max}^{(g)})^2(e_{\max}^{(g)} - 1)}{1 - 4\beta^2(\eta^{(g)})^2e_{\max}^{(g)}(e_{\max}^{(g)} - 1)} - 1 < 0. \quad (27)$$

$$1 - 4\beta^2(\eta^{(g)})^2e_{\max}^{(g)}(e_{\max}^{(g)} - 1) > 0. \quad (28)$$

Thus, we get the condition:

$$\eta^{(g)} < \frac{1}{2\beta\sqrt{e_{\max}^{(g)}(e_{\max}^{(g)} - 1)}}. \quad (29)$$

Assume there exists a set of constants $\Lambda^{(g)}$, $\forall g$, where:

$$\frac{4(\eta^{(g)})^2\beta^2(\Theta^{(g)})^2(e_{\max}^{(g)}(e_{\max}^{(g)} - 1))}{1 - 4(\eta^{(g)})^2\beta^2e_{\max}^{(g)}(e_{\max}^{(g)} - 1)}\zeta_1 < \Lambda^{(g)} < 1, \quad \Lambda^{(g)} < \zeta_1 \quad (30)$$

Then we will have

$$\eta^{(g)} \leq \frac{\sqrt{\Lambda^{(g)}}}{2\beta\sqrt{(\zeta_1 + \Lambda^{(g)})e_{\max}^{(g)}(e_{\max}^{(g)} - 1)}} \quad (31)$$

and

$$\frac{1}{(1 - 4(\eta^{(g)})^2\beta^2e_{\max}^{(g)}(e_{\max}^{(g)} - 1))} \leq \frac{\zeta_1 + \Lambda^{(g)}}{\zeta_1} \quad (32)$$

Note that the condition in (31) is stricter than (29). Putting altogether, we get

$$\begin{aligned} & \|\nabla F^{(g)}(\mathbf{w}^{(g)})\|^2 \\ & \leq \frac{2(F^{(g)}(\mathbf{w}^{(g)}) - \mathbb{E}_g[F^{(g)}(\mathbf{w}^{(g+1)})])}{\eta^{(g)}(1 - \Lambda^{(g)})} \\ & \quad + \frac{4\beta(\Theta^{(g)})^2\eta^{(g)}}{1 - \Lambda^{(g)}} \sum_{k \in \mathcal{K}^{(g)}} \frac{(\tilde{\sigma}_k^{(g)})^2}{D_k^{(g)}} e_k^{(g)} \left(1 - \frac{B_k^{(g)}}{D_k^{(g)}}\right) \frac{1}{B_k^{(g)}} \\ & \quad + \frac{2\beta^2(\eta^{(g)})^2}{D^{(g)}(1 - \Lambda^{(g)})} \sum_{k \in \mathcal{K}^{(g)}} (e_k^{(g)} - 1) \frac{\zeta_1 + \Lambda^{(g)}}{\zeta_1} \left(1 - \frac{B_k^{(g)}}{D_k^{(g)}}\right) \frac{(\Theta^{(g)})(\tilde{\sigma}_k^{(g)})^2}{B_k^{(g)}} \\ & \quad + 4\beta^2(\eta^{(g)})^2(e_{\max}^{(g)})(e_{\max}^{(g)} - 1) \frac{\zeta_2}{1 - \Lambda^{(g)}} \frac{(\zeta_1 + \Lambda^{(g)})}{\zeta_1} \end{aligned}$$

Summing from 1 to G and dividing by G and applying $\frac{\zeta_1 + \Lambda^{(g)}}{\zeta_1} < 2$ lead to

$$\begin{aligned} & \frac{1}{G} \sum_{g=1}^G \|\nabla F^{(g)}(\mathbf{w}^{(g)})\|^2 \\ & \leq \frac{1}{G} \sum_{g=1}^G \frac{2(F^{(g)}(\mathbf{w}^{(g)}) - \mathbb{E}_g[F^{(g)}(\mathbf{w}^{(g+1)})])}{\eta^{(g)}(1 - \Lambda^{(g)})} \end{aligned}$$

$$\begin{aligned}
& + \frac{1}{G} \sum_{g=1}^G \frac{4\beta(\Theta^{(g)})^2(\eta^{(g)})}{1 - \Lambda^{(g)}} \sum_{k \in \mathcal{K}^{(g)}} \frac{(\tilde{\sigma}_k^{(g)})^2}{D_k^{(g)}} e_k^{(g)} \left(1 - \frac{B_k^{(g)}}{D_k^{(g)}}\right) \frac{1}{B_k^{(g)}} \\
& + \frac{1}{G} \sum_{g=1}^G \frac{4\beta^2(\eta^{(g)})^2}{D^{(g)}(1 - \Lambda^{(g)})} \sum_{k \in \mathcal{K}^{(g)}} (e_k^{(g)} - 1) \left(1 - \frac{B_k^{(g)}}{D_k^{(g)}}\right) \frac{(\Theta^{(g)})(\tilde{\sigma}_k^{(g)})^2}{B_k^{(g)}} \\
& + \frac{1}{G} \sum_{g=1}^G 8\beta^2(\eta^{(g)})^2 (e_{\max}^{(g)})(e_{\max}^{(g)} - 1) \frac{\zeta_2}{1 - \Lambda^{(g)}}
\end{aligned}$$